AD-A134 125 REAL TIME OPTICAL INTERFEROMETRIC IMAGE ADDITION AND SUBTRACTION BY WAVE POLARIZATION(U) LUMIN INC TUSCALOOSA AL H LIU 15 OCT 81 LUMIN-81-01 1/1

UNCLASSIFIED DAAH01-81-C-B120 F/G 20/6 NL

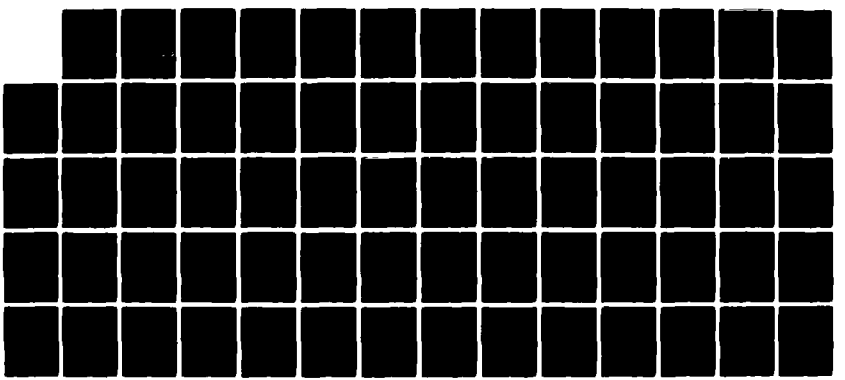

END

DATE FILMED

DTIC

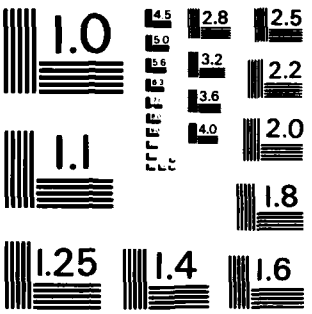

LUMIN

A

Final Report

on

Contract

No. DAAH01-81-C-0120

Real Time Optical Interferometric Image Addition and Subtraction by Wave Polarization

by

Hua-Kuang Liu

Prepared for

U. S. Army Missile Command
Redstone Arsenal, Al. 35898

October 15, 1981

LUMIN Report No. 81-01

Lumin, Inc.
P.O. BOX 5620 TUSCALOOSA, ALABAMA 35401

DISCLAIMER NOTICE

THIS DOCUMENT IS BEST QUALITY PRACTICABLE. THE COPY FURNISHED TO DTIC CONTAINED A SIGNIFICANT NUMBER OF PAGES WHICH DO NOT REPRODUCE LEGIBLY.

REAL-TIME OPTICAL INTERFEROMETRIC IMAGE ADDITION AND SUBTRACTION BY WAVE POLARIZATION

ABSTRACT

A real-time coherent optical interferometric image addition and subtraction system based on a technique similar to an earlier work by Kunstmann and Spitschan[6] is extensively investigated. Theoretical analysis of the system has been compared with experimental data obtained. Distortion and resolution power of the system with respect to the size and positions of the input images have been analyzed in detail.

TABLE OF CONTENTS

REAL-TIME OPTICAL INTERFEROMETRIC IMAGE ADDITION AND SUBTRACTION BY WAVE POLARIZATION

1. Introduction

Optical image addition and subtraction by holography[1,2] and interferometry[3,4] have been investigated by various researchers. In most of the interferometric methods, complex amplitudes of two images from different light paths of an interferometer are recombined by a grating or by an ordinary holographic beam splitter. By introducing a phase difference of π into one of the paths, the subtraction between the two images can be achieved. However, in the method used by Kunstmann and Spitschan[5], an analyzer was used to produce opposite phases for the two spatially separated images and a Wollaston prism was used for the recombination of the two images. The method is comparatively simpler and offers the following advantages. It is easier to change the phase difference between the imaging paths of the two images since this can be achieved by simply rotating the analyzer. The imaging paths of the two images are relatively closer to each other than those in the system using a Mach-Zehnder interferometer.[4] Hence the method is less vulnerable to environmental vibrations. Furthermore, no holographic beam splitters or gratings are required. The birefringent Wollaston prism is commercially available. However, although Kunstmann and Spitschan[5] reported that subtraction has been performed in an area of 3mm by 3 mm in their experiment, no theoretical analysis of their experimental results with regard to the various optical components such as the lens and Wollaston prism have been given. For example, they have not taken the aberrations of the Wollaston prism and the precision of the coincidence of the two images into

consideration. The spherical aberration of the Wollaston prism in their system can introduce errors in the subtraction and addition and the light efficiency in the system is low. For this reason, we have investigated an improved system. The details of the theory, experimental results, and experimental data analysis of the improved system are described in the following Sections.

II. Theoretical Discussion

The basic principle of the technique of performing real-time image subtraction and addition using polarization modulation can be illustrated with the assistance of Fig. 1. Besides ordinary polarizers, a special polarization element used is called a Wollaston prism.

In Fig. 1, S is a coherent point light source, C is a collimator, S_1 and S_2 are two transparencies with their amplitude transmittances $S_1(x_1,y_1)$ and $S_2(x_1,y_1)$ representing respectively the two input signals being processed. The center of S_1 is located at $(-x_0,0)$ and that of S_2 is at $(x_0,0)$ in the input plane I_1, and both of them are inclined at an arc angle θ to the z-axis as shown in Fig. 1. The input plane I_1 is located at the front focal plane of the lens L_1 and the output plane of the system is at the back focal plane of lens L_2. P is a polarizer and AN is an analyzer. P_1 and P_2 are two modulation polarizers located in front of the input transparencies S_1 and S_2 respectively. The unit-vectors along the directions of the principal transmittance of P, P_1, P_2, and AN, represented by $\vec{P}$, $\vec{P}_1$, $\vec{P}_2$, and $\vec{A}$ respectively, are shown in Fig. 2. W is a Wollaston prism which is located at the vicinity of the back focal plane of L_1 and the front focal plane of L_2 and has its two optical axes parallel to P_1 and P_2 respectively.

For simplicity, we shall assume that the two lenses L_1 and L_2 have the same focal length f and have perfect image formation properties with

the input plane I_1 and output plane I_2 as a pair of conjugate planes. Since the spherical waves radiated by the points at the plane I_1 are transformed into plane waves by lens L_1, the Wollaston prism though can introduce distortions but will not induce any other monochromatic aberrations for objects at plane I_1.

The complex, vectorial amplitude distribution of the illuminating light at I_1 may be represented by P. As a result of the polarization modulation of S_1 and S_2, the amplitude distribution I_1 immediately behind the input plane is

$$I_1 = [S_1(x_1+x_0, y_1)\, P_1 + S_2(x_1-x_0, y_1)\, P_2] \qquad (1)$$

If there is no Wollaston prism in the system, the different polarization states of S_1 and S_2 would not affect their image locations, and the two images would still be separated at the output plane I_2. However, when the prism is in place, the situation is different. The Wollaston prism will deflect the light beams passing through it according to the polarization state. As can be seen in Appendix A, the values of the angles of deflection for beams polarized along P_1 and P_2 are both approximately equal to:

$$\epsilon = \tan A\,(n_o - n_e) \qquad (2)$$

where A is the apex angle of the Wollaston prism defined in the Appendix, n_o and n_e are the refractive indexes of the prism corresponding to the ordinary and extraordinary beams respectively. However, the directions of the deflections of these two beams are opposite to each other. Thus, if we adjust the distance x_0 to make the angle of inclination θ be equal to the angle ϵ, the centers of the images of S_1 and S_2 can both be shifted to be on the z-axis in the output plane and hence the two images will

coincide, limited by distortions, with each other (see Appendix A). Apart from an approximately uniform amplitude attenuation and constant phase retardation (see [2A]), T_{12}, start from a complex constant, the output amplitude, O, of the second beam splitter with an analyzer $\vec{A}$ being placed in front of I_2 can be written as:

$$\vec{O} = \frac{\sqrt{2}}{2} [S_1(x_2, y_2) \vec{P}_1 + S_2(x_2, y_2) \vec{P}_2] \quad .$$

When $\vec{AN}$ is placed in front of I_2 as shown in Fig. 1; due to the relationship among $\vec{P}$, $\vec{P}_1$, $\vec{P}_2$ and $\vec{A}$ (Fig. 2), the output becomes

$$\vec{O} = \frac{1}{2} [S_1(x_2, y_2) - S_2(x_2, y_2)] \vec{A} \quad . \tag{3}$$

The image subtraction between S_1 and S_2 can thus be achieved.

Moreover, the flexibility of the proposed system can be seen by the fact that broader image processing capabilities can be attained by simple manipulation of the relative angular positions of $\vec{P}$ and $\vec{A}$. First, we notice that the negative sign in Eq. (3) is caused by a "crossed" polarizer setup, i.e., $\vec{P} \perp \vec{A}$ as shown in Fig. 2. If we rotate $\vec{A}$ by 90°, a parallel polarizer setup is obtained and the output then becomes

$$\vec{O} = \frac{1}{2} [S_1(x_2, y_2) + S_2(x_2, y_2)] \vec{A} \tag{4}$$

and hence image addition can be achieved. Secondly, if a linear combination of the two images is desired, we can simply rotate AN (or P) to obtain the following output,

$$\vec{O} = \frac{\sqrt{2}}{2} [S_1(x_2, y_2) \cos\theta \mp S_2(x_2, y_2) \sin\theta] \vec{A} \tag{5}$$

where θ is the angle between $\vec{A}$ and $\vec{P}_1$ and the "-" and "+" signs correspond

to the geometries shown in Fig. 3(a) and Fig. 3(b) respectively.

The simple and convenient technique for the linear combination of these images has its practical importance. For example, in image subtraction, the two transparencies usually do not have the same transmittance over the supposed-to-be identical portion of the two images due to the differences in emulsions or the exposure and development conditions. Thus, in order to carry out a true subtraction, a "weighted" subtraction or a linear combination is required for the removal of the pseudo-differences.

III. Experimental Results

A. The experimental set-up

The experimental system is optically constructed according to the diagram shown in Figure 1 with slight modifications. A 50 mW He-Ne laser was used as the light source, the polarizer P is placed in the raw laser beam before the collimating lens C. The polarized beam, after being expanded through a pin-hole spatial filter, was collimated by a 6-inch aperture 36-inch focal-length telescopic lens C. It was found that the polarizers P_1 and P_2 were not required. In that case, each input image produces two spatially separated images at the output plane, and the useless one can be easily blocked. The rest of the system remained the same except that the imaging lens L_2 was inserted between the analyzer AN and the final output image I_2. Five different lenses have been used at the position of L_1 for the purpose of finding out the influence of the Fourier transform on the effect of subtraction. The important characteristics of the lenses are listed in Table 1. The Wollaston prism is made of calcite, with its front surface area of 12mm by 10mm, total thickness of 6 mm, and the split angle of 5° (the apex angle A = .245 rad.).

2. Interference fringes resulted from the subtraction of two open spaces.

During the experimental process, the lenses listed in Table I were one by one replaced at L_1 of Fig. 1 and the output image at I_2 of the system was observed closely. When there was no specified image being placed at I_1 plane, the subtraction was performed between two open spaces at I_1 and I_2 of Fig. 1. It has been found that the two possible side-axis orientations of positioning the Fourier transform lens has a significant influence on the result of subtraction. The subtraction between the two open spaces only yields the interference fringes which will be analyzed in the next Section. When the Fourier transform lens is placed with one of its two surfaces facing toward the light source (say Orientation 1) broader interference fringes can be obtained than when the surface is placed facing away from the light source (say Orientation 2). The phenomenon, common to all the lenses listed in Table I, is further illustrated in Figs. 4-9. Figures 4 and 5 present the photographic recordings of the interference fringes where the Fourier transform lens L_1 was placed along Orientation 1 and 2 respectively. The various parts in these Figures indicate the different positions of the Wollaston prism along the optical axis. When the Wollaston prism was placed at position a, the dark fringe has a miximum area in the interference fringe pattern. It can be seen that this is true for Figures 4 and 5. However, the results of Figures 6-9 are photographic recordings of

the interference fringes where L_{II}, L_{III}, L_{IV}, and L_V were placed with orientation 1 and the Wollaston prism was so positioned that the dark fringe is maximized. The b parts of the same figures correspond to the cases when these lenses were placed along Orientation 2 in the system but with the Wollaston prism arbitrarily positioned. It has been found that along Orientation 2, no matter how one adjust the position of the Wollaston prism, there was no way to obtain a greater dark fringe area than those obtained with the lens along Orientation 1.

It is important to note that the dark fringes caused by the destructive interference of the areas in the two open spaces at the input image plane are the useful areas for the performance of the subtraction. Therefore, we have attempted to maximize the dark fringes in the interference fringe patterns created by L_I through L_V each along the two possible axial orientations. The results of computations of the maximum x- and y-dimensions of the dark areas from one of the photographs of Figures 4 through 8 to the best accuracy as one can estimate are listed in Table II. Although the maximum area does not equal to XY for each of the cases listed in Table II, it seems that L_{II} placed along Orientation 1 would yield the maximum area for subtraction in comparision with the other lenses.

C. Results of subtraction between two specific input images -- a penny and a metal washer.

Since L_{II} placed along Orientation 1 has yielded the maximum area of the dark fringe, it was chosen for the Fourier transform lens. Two

input [illegible] penny and a metal washer, are placed respectively at S_1 and S_2 at the input plane I_1, of Fig. 1. A uniform transparent glass plate was placed at I_1 to support the penny and washer. The two objects are attached to the glass plate by double-stick tapes. The diameter of the penny is approximately 19 mm (3/4"). The metal washer has an out side diameter of approximately 9.52 mm (3/8") and a hole in the center of a diameter of about 4.76 mm (3/16"). The photographic recordings showing the subtraction results are presented in Fig. 11. The approximate center-to-center distances between the penny and washer are 70 mm (2 3/4"), 63.5 mm (2 1/2") and 60 mm (2 3/8") for a, b, and c part of the photographs in Fig. 11 respectively. These photographs have illustrated the partial overlapping, just complete overlapping, and total [illegible] position of the washer and the penny in the output plane as a result of the subtraction of the original objects that are placed apart. The dark areas of the outer portion of the washer vividly demonstrated the subtraction phenomenon. The thin hair-line spacing between the outer parts of the penny and the washer is an indication of the resolution of the subtraction. The irregular traces of marks in the lower portion of the penny was caused by the glue left by the penny on the glass plate. It can be seen from the three parts in Figure 11 that the residue glue did not change its position when the penny was moved. The glue mark is also an indication of the resolution of the system.

IV. Data Analysis

In order to understand the subtraction system thoroughly, the interference fringe patterns as shown in Figs. 4-10 require a theoretical interpretation and the degree of accuracy of the subtraction results needs to be analyzed. We shall discuss these two aspects of the system as follows.

A. Interpretation of the interference fringes

The theoretical model that we propose to interpret the interference fringe pattern assumes that all optical components used in our system are optically perfect, i.e., the lenses are free of aberrations. The reason that the fringes appear at the output plane is mainly due to the fact that two different coherent light rays which pass through two different points on the input plane recombine at the output plane [illegible] the effect of the [illegible] the position of the point on the output plane [illegible] the interference pattern at the output plane [illegible] the interference fringes based on the light ray concept. The light ray concept is based on the approximation of geometrical optics, since we assume that the contribution of light diffraction may be neglible in the present case. More details of the model are presented below with the help of some illustrations.

A part of the image processing system of Fig. 1 is shown in more fine details in Fig. 12. Point p_3 is a certain point with coordinates (x_3, y_3) on the output plane. Based on the principle of geometrical optics, it is not difficult to find the locations of the two input plane points p_1 and p_2 that correspond to the output point p_3. Since in the idealized case under the assumption that the system is free of aberrations and diffractions, p_1 (or p_2) and p_3 are a pair of conjugated object/image points. The optical path between p_1 (or p_2) and p_3 can be evaluated along any ray passing through both of them. To be specific, we choose the rays originating from p_1 and p_2 that are parallel to the optical axis before they reach the Fourier transform lens. Hence the two rays would intercept at the back focal point of the lens.

[illegible] an enlarged illustration of the Wollaston prism and the vicinity of the point P_3, Fig. 13, is drawn for the typical paths of the rays that go through the Wollaston prism. From Fig. 13, it can be seen that the path length difference between $P_1P_{1'}$ and P_2P_3 is equal to the path length difference between (BCD-EM) and (EBHJ-EM). Based on this path length difference, we have calculated on a digital computer the interference fringe patterns. Other pertinent data used in the calculations include the wavelength λ = 632.8 nm; the thickness of the Wollaston prism d = 5.0 mm, the apex angle of the Wollaston prism A = 0.245 radians; the ordinary refractive index n_o = 1.6584*; the extraordinary refractive index n_e = 1.4864*. The focal lengths of the Fourier lens and the focusing lens are both equal to f = 750 mm; the ranges of the position of the point P_3 (x_3, y_3) are -100 mm < x_3 < 100 mm; y_3 = -166.7 < y_3 < 166.7 mm; the location of y_3 varies with Δy_3 = 2 mm and Δy_3 = 3.33 mm; and finally, the distance between the front surface of the Wollaston prism and the back focal point F of the Fourier transform lens is taken as a parameter which varies from 1.75 mm to 2.00 mm with a step increment of 0.01 mm to account for the manual adjustment of the Wollaston prism in the system.

The results of the calculations are plotted by the computer and shown in Fig. 14 where the interference fringes are represented by dots and B's. The dots denote that the absolute value of a fraction of the path length difference introduced by the Wollaston prism at P_3 is less than $\lambda/4$ or greater than $3\lambda/4$ and the letter B denotes that the absolute

* These indices are for wavelength λ = 589.3 nm; for λ = 632.8 nm the calculated patterns would be slightly different.

value of the path length difference is between $\frac{\lambda}{4}$ and $\frac{3\lambda}{4}$. Thus, if the analyzer is set, it does not introduce any additional phase difference. The dots stand for the 'bright' fringes, and the 'E's stand for 'dark' fringes. If the analyzer is fixed, additional phase differences will be introduced. The computer simulated results in Appendix E.

Finally, we can see from Fig. 14 that around $\Delta = 1.5$ mm the width of the fringes is at minimum and the relatively uniform area of the dark fringe is at its maximum. The maximum dark area is best for performing image subtraction. The theoretically predicted phenomenon has been also qualitatively verified by the experimental results. Any quantitative differences between the computed and experimental data probably is caused by the imperfectness of the Wollaston prism and the aberrations of lenses. The phenomenon that the fringe patterns are different for a certain lens at the two different orientations can also be explained by the fact that the aberration is dependent on the orientation.

. The distortions at the output plane.

Due to the fact that the angular deflection of the light ray by the deflecting plane usually varies with the incident angle at the front surface of the prism, the images superposed at the output plane cannot totally coincide with each other. Both images suffer from different amount of distortions. The resolution power of the subtraction technique is limited by these distortions. In the following, we estimate how serious the distortion is and try to find out the optimum positions of placing the two input images where the distortions can be minimized. For simplicity, the calculation is done only for one-dimensional case. We assume that the Wollaston prism has the same parameters as those in the A part of this

Section 3.2 that both the Fourier lens and the imaging lens have the same focal length $f = 1$ (arbitrary unit), then the magnification of the whole system is 1.

The calculation is based on the configuration as shown in Fig. 15. First we choose a point C_3 on the output image and then trace back along the geometrical optical paths to two corresponding points C_1 and C_2 on the two input transparencies. We shall call the points C_1, C_2, and C_3 the centers of the respective images. Likewise, for any point P_3 on the output, the corresponding input image points P_1 and P_2 on the input can also be found. We further let $H_1 = \pm|\vec{C_1P_1}|$, $H_2 = \pm|\vec{C_2P_2}|$, and $H_3 = \pm|\vec{C_3P_3}|$ where the positive sign is chosen if the vector is parallel to the positive x-axis. If there is no distortion, $H_1 = H_2 = H_3$. The difference $H_2 - H_1$ or $H_3 - H_2$ can be used to measure the amount of distortion and the difference $H_2 - H_1$ can be used to determine the resolution of subtraction. For example, according to our calculated results, if the point at the intersection of the output plane and the optical axis is chosen as C_3, then C_1 and C_2 will have their x-coordinate values of 0.1000 and 0.0969 respectively, where all units are considered to be the same as that of the focal length. An output image point P_3 with $H_3 = 0.1000$ has its corresponding object points P_1 with $H_1 = 0.1030$ and P_2 with $H_2 = 0.1061$. In this case, the difference $H_1 - H_2 = 0.0031$ is the minimum resolvable distance when the image height is around 0.1. The overall resolution data are illustrated further by two additional figures. Figure 16 is a plot of $H_2 - H_1$ versus H_3 when C_3 is located on the axis. It can be seen that, for the same value of $|H_3|$ and $|H_3| = 0.01$, the difference $H_2 - H_1$ is much greater for positive H_3 than for negative H_3. Thus, in order to minimize distortion and simultaneously maximize the size of the image to be subtracted one has to choose an optimum set of centers of images (C_1, C_2, C_3)

For example, if the maximum tolerable difference $(H_2 - H_1)$ is 0.001 and we place the upper end point of each of the input images 0.04 above its center ($\lambda = 0$), the total height of the image can be subtracted would be 0.04 - (-0.16) = 0.19. If instead, when the middle point of the image is placed at the 'center', the total height of the image that can be subtracted within the tolerance is then reduced to 0.04 - (-0.04) = 0.08. Figure 17 shows a different case in which the point C_3 is not located at the optical axis but at $\lambda_3 = -0.05$. Then it can be seen that the values of $H_2 - H_1$ are almost distributed symmetrically around the center ($H_3 = 0.1$). With the maximum tolerable $H_2 - H_1$ is 0.001 and the middle points of the two ray transmittances are placed at the centers C_1 and C_2, the total height of H_3 image is reduced to (0.1) - (-0.08) = 0.18. Note that in this case the distortion around the center changes very slowly and have negligible values. It is also interesting to find out the relative distortion as defined by $\left|\frac{H_2 - H_1}{H_3}\right|$ excluding $H_3 = 0$. Two additional figures corresponding to the above-described two cases are plotted and shown in figures 18 and 19 respectively. We can see that for the first case (C_3 located on axis) the relative distortion is greater at the vicinity of the center than at the lower part of the image. For the second case (C_3 at $\lambda_3 = -0.05$), the minimum relative distortion appears at the vicinity of the center. The total height for the first case within the tolerance of $\left|\frac{H_2 - H_1}{H_3}\right| = 1$ is about (-0.04) - (-0.16) = 0.12 while the total height for the second case is about 0.06 - 0.04 = 0.14. The computer programs for the calculations are listed in Appendix C and D respectively.

V. Conclusions

We have presented the principle, experimental data, and data analysis of a real-time image subtraction technique by using the properties of wave polarization. The theoretical analysis predicts that interference fringes should be produced in the system and the experimental data demonstrated the phenomenon. The dark (or destructive interference) portion of the fringes can be used for performing image subtractions. The maximum area that can be used for subtraction in the system we constructed is about 26 mm x 18 mm, which is almost one to two orders of magnitude greater than that reported earlier by Lohmann and Paris. In addition, in the present system, the object and the image have the same light efficiency in comparison with those of Lohmann and Paris. A detailed calculation of the distortion of the image due to aberrations also has revealed the optimum positions where the input mask should be placed at the input plane when the tolerance of the distortion of distortion error is set. From the experimental data, it seems that the Fourier lens with the smallest D/F yeilds the greatest usable subtraction area. This is expected since in general lenses with greater f-number have less aberrations.

With regard to future work, it seems that two feasible ideas should be investigated. One is to incorporate the subtraction technique in an electro-optical system that includes the use of a Hughes liquid crystal light valve (LCLV) for real-time image subtraction in a continuous mode. The other is to apply the Wollaston prism for performing real-time pseudo-color image subtraction or additions. Both of these ideas could lead to important practical applications.

APPENDIX A

THE FUNCTION OF A WOLLASTON PRISM

Based on the nature of a Wollaston prism, light beam traveling through the prism will gain an amount of path-length according to the beam's orientation of polarization. To illustrate the effect, a x-z plane cross-section of a Wollaston prism which consists of two triangle prisms is shown in Fig. A1. Each triangle has the apex $A = \tan^{-1}(t/H)$, where t is the thickness and H is the height of the prism. The two triangle prisms are made of the same kind of birefringent crystal but have different optic axes. For our purpose, if the crystal is a "negative" one, such as the calcite, the optic axis of the left half, as shown by "·" in Fig. A1, is parallel to x-axis (or P_1) and that of the right half (by "|"), is parallel to y-axis (or P_2). Thus, for the light beam polarized along P_2, the path length increment $\Delta_1(x)$ is approximately,

$$\Delta_1(x) \approx (\tfrac{t}{2} + x\tan A)(n_o - 1) + (\tfrac{t}{2} - x\tan A)(n_e - 1)$$

$$= [(n_o + n_e)t/2 - t] + x(n_o - n_e)\tan A \quad . \tag{A1}$$

Similarly, for the light beam polarized along P_1, the increment $\Delta_2(x)$ can be written as

$$\Delta_2(x) \approx [(n_o + n_e)t/2 - t] - x(n_o - n_e)\tan A \quad . \tag{A2}$$

Based on the assumptions represented by equations (A1) and (A2), two important conclusions can be deduced. First, any plane wave after

traveling through a Wollaston prism will be deflected by an angle α, which is approximately equal to $(n_o - n_e)\tan A$. Because we have $n_o > n_e$ for a negative crystal, α has a positive value, i.e., all plane waves coming from the points of S_1 will be deflected downward by an angle α since they are polarized along P_1. The image of S_1 at the output plane will then also be moved downward. It will be centered on the z-axis, if we make $f = z$. Since all light waves from S_2 are polarized along P_2, the image of S_2 will move upward and coincide with the image of S_1.

Furthermore, the amplitude distribution at the Wollaston prism will not affect the calculated path length difference, yet, due to the focusing effect of L_1, a Wollaston prism of relatively small aperture can be used.

```
      1              REAL L,L1,L2,L3,L4
      2              CHARACTER*1 MP(101,101)
      3              WRITE(6,*)'S,L'
      4              READ(5,*)S,L
      5              AF=2.*L
      6              DO 9 I=1,101
      7              WRITE(6,*)I,2*I
      8              FORMAT(1X,I3,1X,A1,I3,1X,A1,I3,1X,A1,I3,1X,A1)
      9              M=0
     10              M=M+1
     11              ALPHA=(M-1)*.5
     12              S2=SQRT(1.+ALPHA**2)
     13              C1=1./S2
     14              S1=ALPHA/S2
     15              D=S1/C1+1.
     16              X3=(L-S1)/2.
     17              Y3=X3/C1+1
     18              Y3=(L-S1)/3.+1.5
     19              S2=SQRT(X3**2+Y3**2-2.*X3*Y3*C1)
     20              AL3=X3/S2
     21              BT3=Y3/S2
     22              GM3=ACOS(-C1)
     23              DO 51 I=1,2
     24              RM1=RM(I)*(M-1)*(RM(2)-RM(1))
     25              RM2=RM(I)*(M-1)*(RM(2)-RM(1))
     26              IF(BT3)10,9,10
     27          9   BT2=0
     28              AL2=AL3/RM2
     29              GM2=SQRT(1.-AL2**2)
     30              C6=AL2*C3+GM2*S4
     31              C7=SQRT(1.-C6**2)
     32              C8=RM2*C7/RM1
     33              C9=SQRT(1.-C8**2)
     34              C10=C9/C4
     35              C11=C3/C4
     36              C12=0.
     37              C13=0.
     38              GO TO 11
     39         10   C1=SQRT(1.-GM3**2)/((RM2**2/RM1-1.+2.*S3/BT3)**.5)
     40              BT2=SIGN(C1,BT3)
     41              AL2=AL3*BT2/BT3
     42              AGM2=1.-AL2**2-BT2**2
     43              IF(AGM2.LT.0..OR.AGM2.GT.1.)GO TO 50
     44              GM2=SQRT(AGM2)
     45              C6=AL2*C3+GM2*(A)/BT2
     46              S6=AL2*S3+AL3*C4
     47              C7=SQRT(1.-C6**2)
     48              C8=RM2*C7/RM1
     49              C9=SQRT(1.-C8**2)
     50              C10=C9/C4
     51              C11=C3/C4
     52              C12=1.-C11/(1+A)
     53              C13=(1.-C11*(1+A))
     54         11   S1=S2*C12+C13*(A)
```

```
     55              IF(S1)71,72,72
     56         71   WRITE(6,*)'S1<0',S1
     57              GO TO 50
     58         72   S1=SQRT(S1)
     59              IF(AL2-C3)  23,23,24
     60         23   AL1=(C11*S3+C13)*(1-C1)+C1
     61              IF(AL1-C3)  25,25,24
     62         25   WRITE(6,*)I,M,AL1,AL2,AL3,BT2,BT3,GM3
     63              GO TO 5
     64         24   AL1=S3*(C11*(1-C8)+C8)
     65              IF(AL1-C3)  26,26,27
     66         26   BT1=S1*AL1+C12
     67              C14=C10-C11*AL1
     68              S14=1.- M1**2*(1.- C14**2)
     69              IF(C14)27,28,28
     70         27   WRITE(6,*)I,M,AL1,AL2,AL3,BT1,BT2,BT3,GM3
     71              GO TO 5
     72         28   IF(C20-1.)29,29,30
     73         29   S20=SQRT(C2 )
     74              IF(AL1)32,32,31
     75         30   AL1=1.
     76              BT1=RM1*BT1
     77              GO TO 33
     78         32   C21=SQRT(1.-GM3**2)/(1.+(BT1/AL1)**2)
     79              AL1=SIGN(C21,AL1)
     80              BT1=AL1*BT1/AL1
     81         33   L=BT1/GM3
     82              X3=AL1*L1
     83              Y3=BT1*L1+L
     84              Z1=G-1*L1
     85              L2=(X3**2+Z1**2)**.5
     86              X2=L2*AL2+X1
     87              Y2=L2*BT2+Y1
     88              WRITE(6,*)M,I,AL1,AL2,AL3,BT1,BT2,BT3,GM3,L1,L2,L3,L4
     89         50   CONTINUE
     90              CALL SYMBOL(X1,Y1,.2,'1',0.,1)
     91              AL3=ABS(AL3)
     92              IF(BT3)52,52,53
     93         52   BT3=-BT3
     94              GO TO 54
     95         53   AL3=-AL3
     96         54   CONTINUE
     97              CALL PLOT(X3,Y3,3)
     98              CALL SYMBOL(X3,Y3,.2,'2',0.,1)
     99              CALL PLOT(0.,0.,3)
    100              CALL SYMBOL(0.,0.,.2,'3',0.,1)
    101              ELSE
    102              CALL SYMBOL(1.,1.,.2,'4',0.,1)
    103              CALL SYMBOL(10.,-1.,.2,'5',0.,1)
    104              STOP
    105              END
```

```
C
C*****12345678901234567890123456789012345678901234567890123456789012
      REAL H(2),F1(2),F2(2),F3(2)
      CHARACTER*1 A(100)
      DO 10 J=1,100
   10 A(J)=' '
      DO 30 J=1,2
      J1=10-5*(J-1)
      CALL F1(J1,F)
      F1(J)=F(1)
      F2(J)=F(2)
      F3(J)=(J1-10)*.01
   30 WRITE(6,12)
   12 FORMAT('1',////15X,' ')
      PRINT*,'GENIUS:  A:',F3(J),'B:',F1(J),'C:',F2(J)
      WRITE(6,40)
   40 FORMAT(////19X,'3',16X,'1',14X,'2',14X,'3',14X,'6',14X,'5',/,
     +'0',8X,'(',F5.3,')',2X,'1',/,19X,6('1',10('-')),'1',5('-'))
      DO 20 K=1,51
      CALL F1(K,F1)
      F1=F1(1)-F1(2)
      F2=F2(1)-F2(2)
      F3=F3*1.01
      F1=F1*5
      A(K)='*'
      WRITE(6,50) K,F1,F2,F3
   50 FORMAT(I3,3F10.4)
      A(K)=' '
      CONTINUE
      A(1)='*'
      A(51)='*'
   20 CONTINUE
      STOP
      END
```

```
      SUBROUTINE F1(K,F)
      REAL H(2),F3(2)
      A=.245
      H0=1.0504
      H1=1.0504
      A=A-(K-1)*.01
      F3=A*A*(H1-H0)
      DO 10 J=1,2
      H(J)=H0+(J-1)*(H1-H0)
   10 F(J)=H(J)*(1-H(J))*(F3-F(J))
      F(J)=-H(1)*(1-H(1))*(F3-A*ASIN(SIN(F3)/H(2))/H(1))
      F(J)=F(J)*H(J)/(1-H(J))
      RETURN
      END
```

```
```

REFERENCES

1. J. [illegible], G. W. Stroke, R. Restrick, A. Funkhouser, and [illegible], Phys. Letters, 18, [illegible] (1965).

2. [illegible], M. A. Monahan, and J. F. Bryant, Appl. Opt. 10, 1[illegible] (1971).

3. S. [illegible], S. K. Yao, and A. G. Milnes, J. Opt. Soc. Am., [illegible] (1970).

4. K. Matsuda, N. Takeda, T. Tsujiuchi, and M. Shinoda, Opt. Commun., 3, 425 (1971).

5. P. Kaufmann and H. J. Spitschan, Opt. Commun., 4, 166 (1971).

6. J. F. Ebersole, Opt. Engr., 14, 136 (1975).

TABLE I. Characteristics of the five lenses used in the following experiments described in Figure 1.

Lens No.	Focal Length f (cm)	Diameter of Aperture D (cm)	D/f
L_I	48.25	9.525	0.197
L_{II}	76.2	10.16	0.133
L_{III}	76.2	15.24	0.2
L_{IV}	30.48	4.08	0.134
L_V	76.2	10.16	0.133

Table II. Measured [illegible] x and y dimensions (denoted by X and Y respectively and in units of mm) of two dark fringes with [illegible] fringes placed along a certain axial orientation.

Lens A	[illegible]	Orientation	X	Y
		1	10.1	8.1
		2	11.9	2.5
		1	[illegible]	[illegible]
		1	12.7	[illegible]
		2	[illegible]	[illegible]
		1	[illegible]	[illegible]
		1	18.2	11.5

FIGURE CAPTIONS

1. A diagram of the polarization modulation white-light image subtraction system.

2. Principal transmittance unit-vectors of the polarizers P, P_1, P_2 and the analyzer A.

3. Principal transmittance unit-vectors of P, P_1, P_2 and A for the linear combination of two images.

4. Photographs of interference fringes with L_I along Orientation 1 and the Wollaston prism at positions a and b.

5. Photographs of interference fringes with L_I along Orientation 2 and the Wollaston prism at positions a, b, c, and d.

6. Photographs of interference fringes with (a) L_{I_1} along Orientation 1 and (b) L_{I_2} along Orientation 2.

7. Photographs of interference fringes with L_{III} along Orientation 1 (a) and Orientation 2 (b).

8. Photographs of interference fringes with L_{I_3} along Orientation 1 (a) and Orientation 2 (b).

9. Photographs of interference fringes with L_V along Orientation 1 (a) and Orientation 2 (b).

10. Photographs of output interference fringes with L_{I_1} placed along Orientation 1 and the Wollaston prism placed at four different positions a, b, c, and d along the axis. No specific images were placed at the input plane of the system.

11. Photographs of the subtraction between a penny and a metal washer with the distance of separation between the two images varied. L_{II} was placed in the system along Orientation 1 and the Wollaston prism was placed at position a as shown in Fig. 10.

12. Light rays originating from points p_1 and p_2 at the input plane reaching the point p_3 at the output plane through the Wollaston prism.

13. The detailed paths of the light rays passing through the Wollaston prism.

FIGURE CAPTIONS (Cont'd)

14. Theoretically computed interference fringe patterns versus the on-axial position of the Wollaston prism.

15. Relative positions of p_1 and p_2 at the input plane and p_3 at the output plane for the computation of image distortion.

16. A plot of $H_2 - H_1$ versus H_3 with C_3 located on-axis.

17. A plot of $H_2 - H_1$, versus H_3 with C_3 located off-axis.

18. A plot of $\log (|H_2 - H_1|/H_3)$ with C_3 located on-axis.

19. A plot of $\log (|H_2 - H_1|/H_3)$ with C_3 located off-axis.

A1. A x-z plane cross-sectional view of a Wollaston prism.

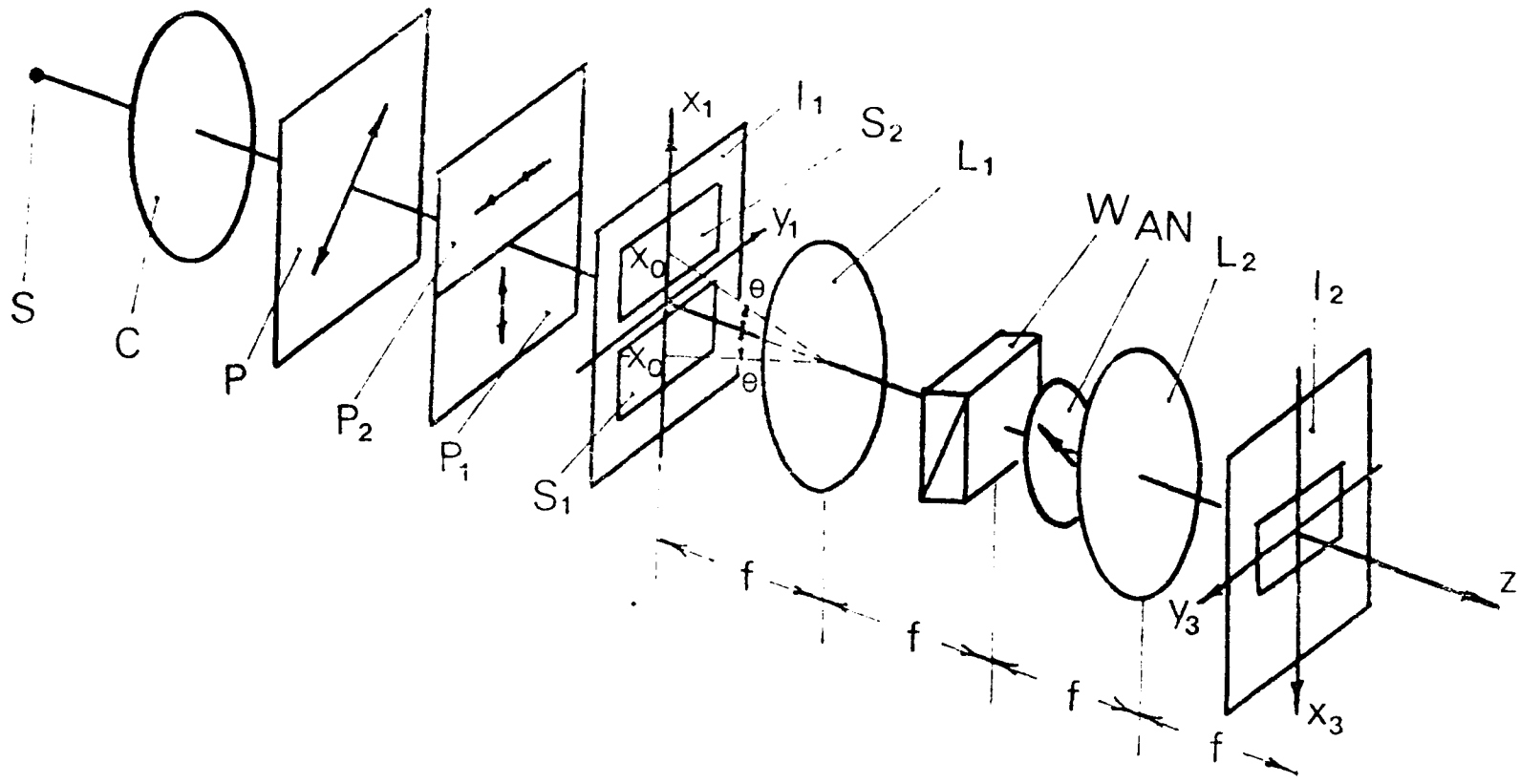
S
C
P
P2
P1
S1
x1
I1
S2
L1
y1
xo
xo
θ
θ
WAN
L2
I2
f
f
f
f
y3
z
x3

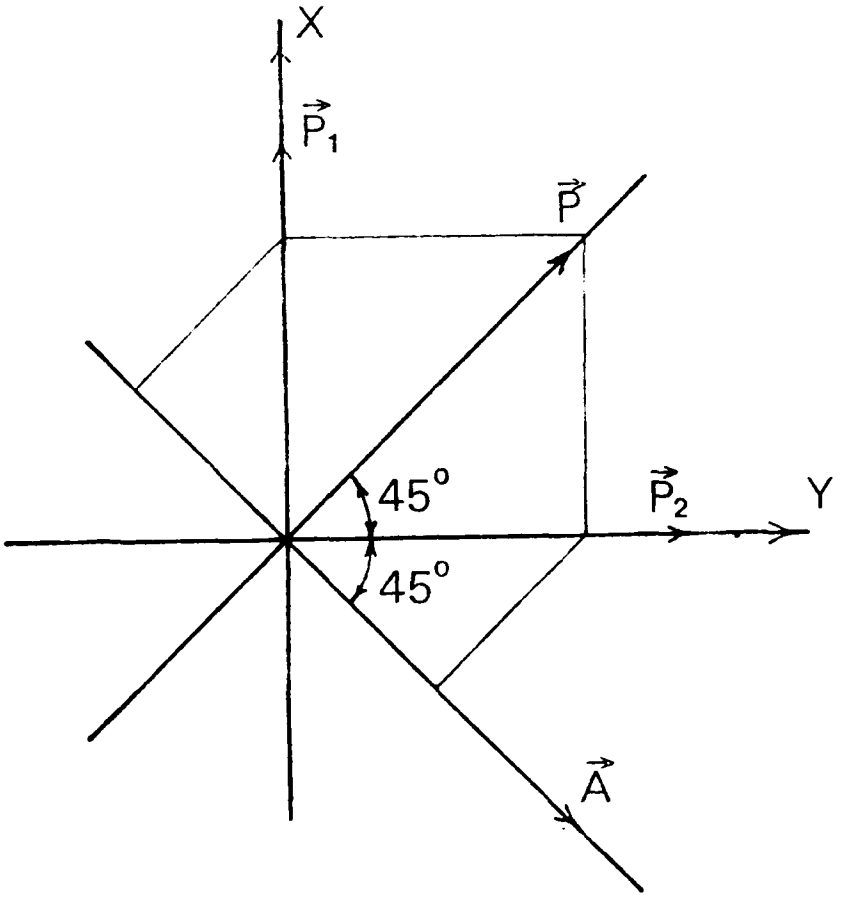
X
$\vec{P}_1$
$\vec{P}$
45°
$\vec{P}_2$
Y
45°
$\vec{A}$

(a)

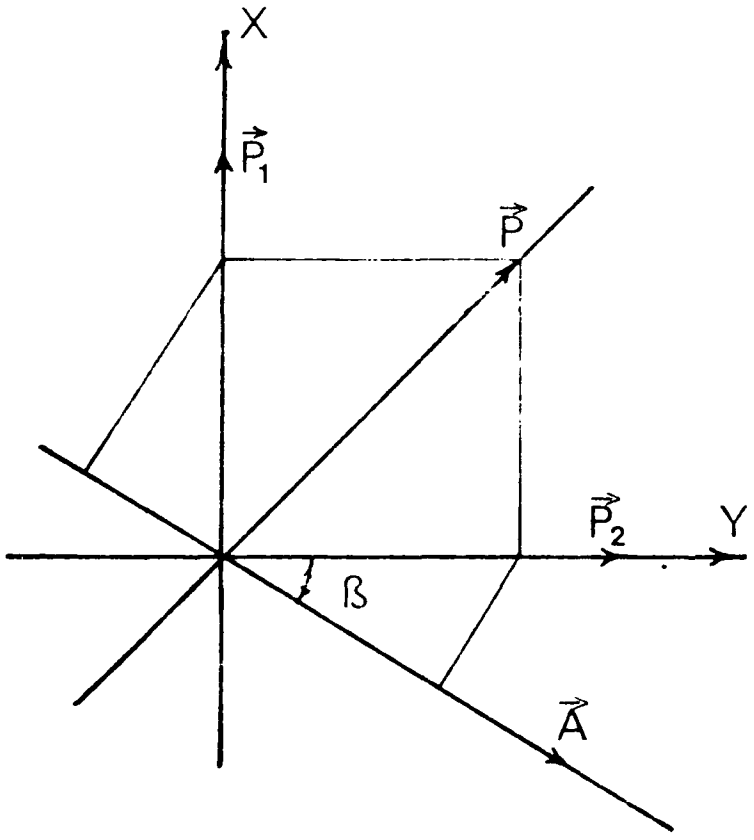

(b)

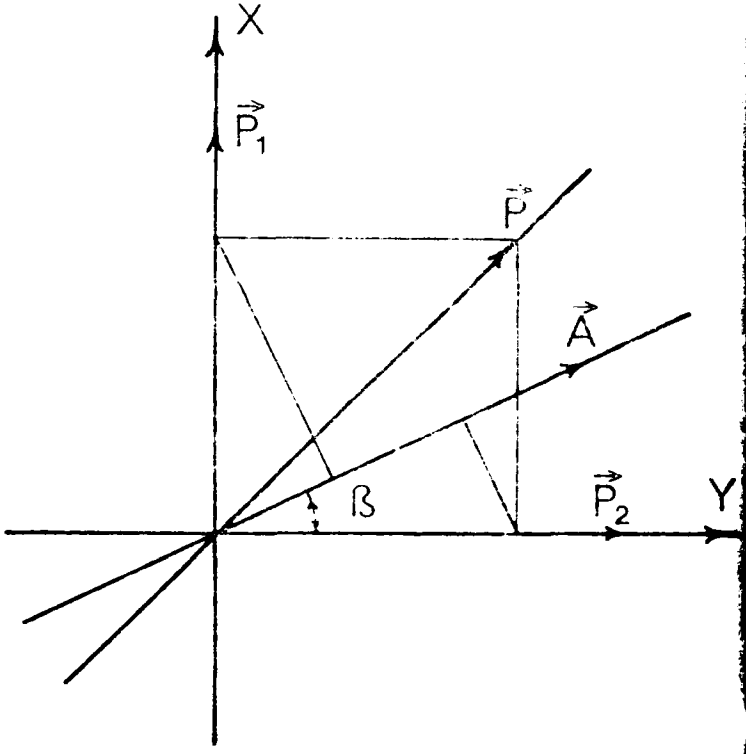

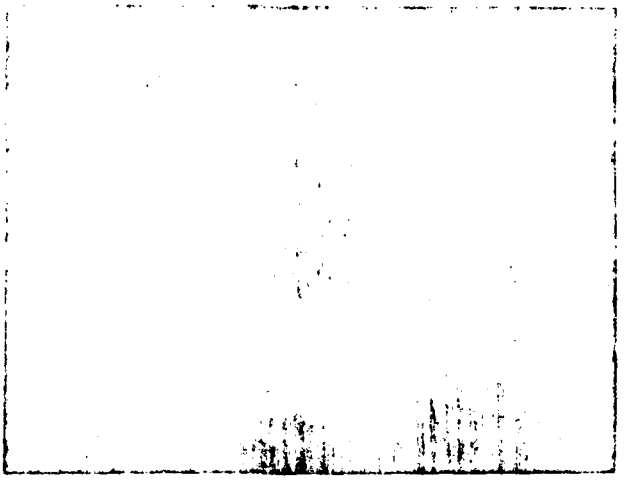

a

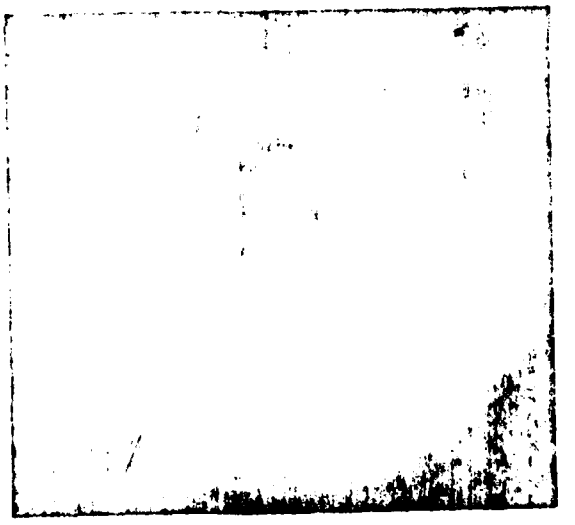

b

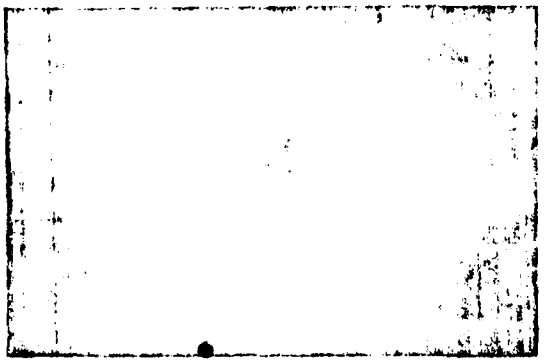

a

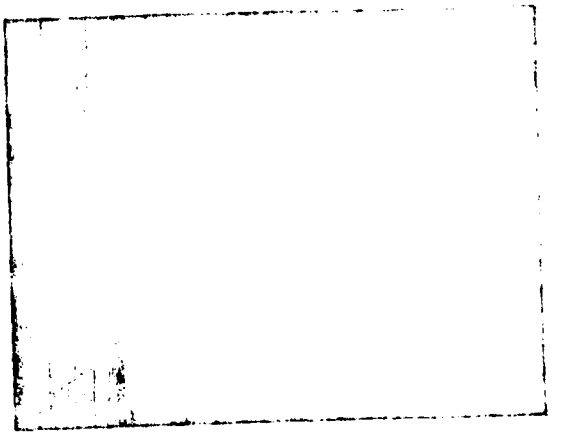

b

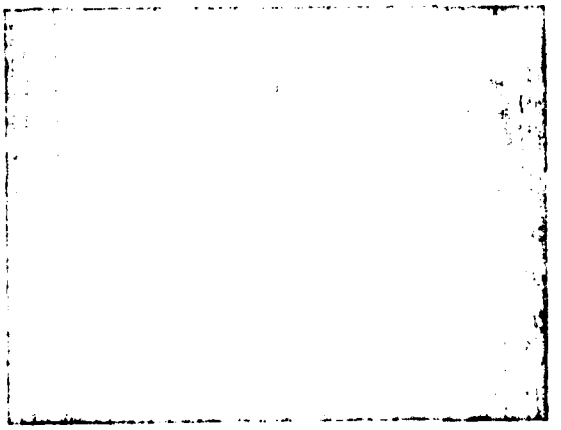

c

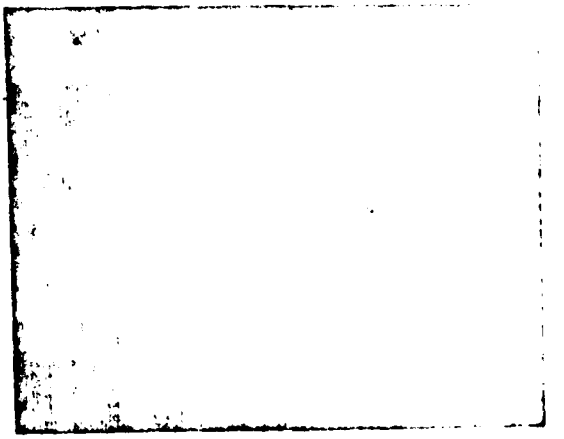

d

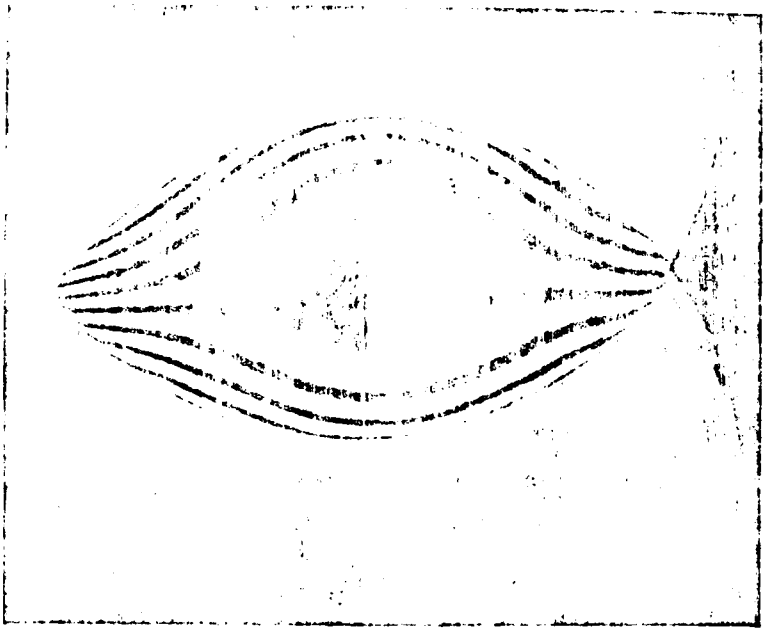

a

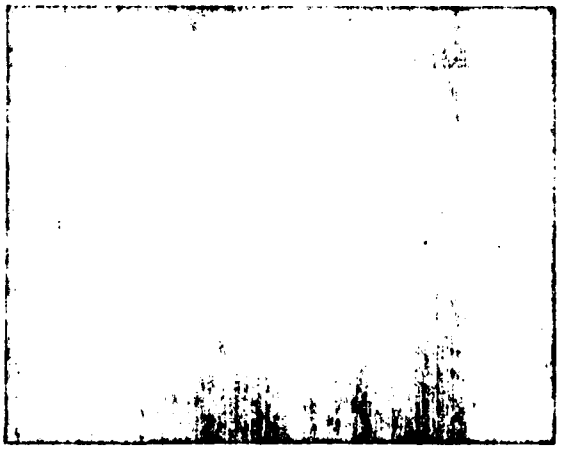

b

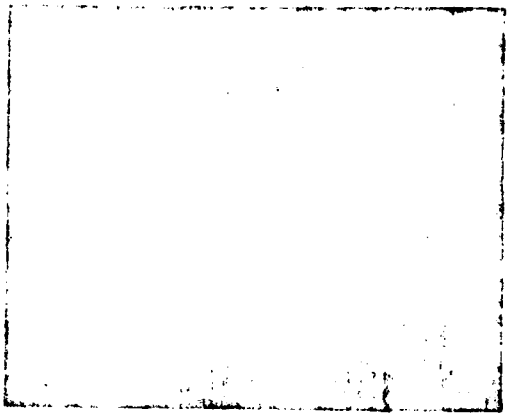

a

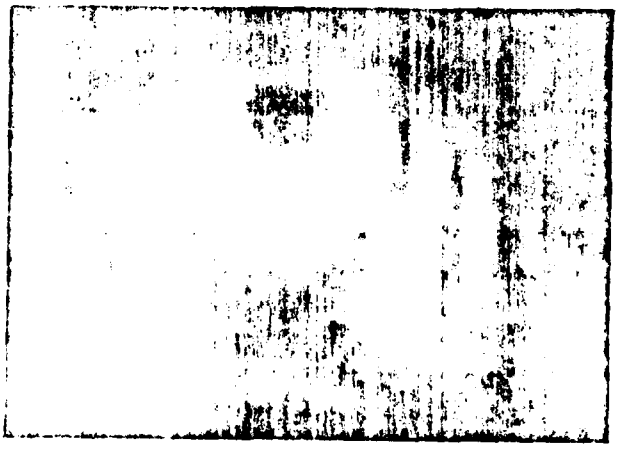

b

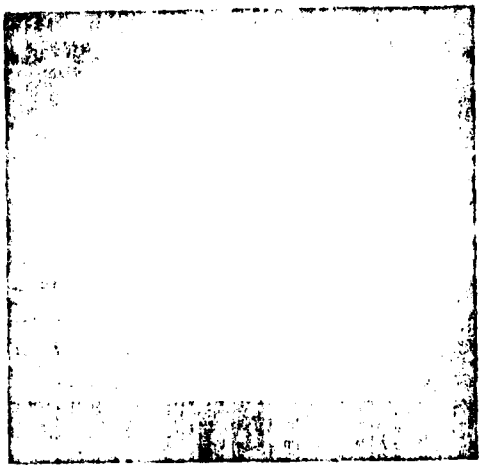

a

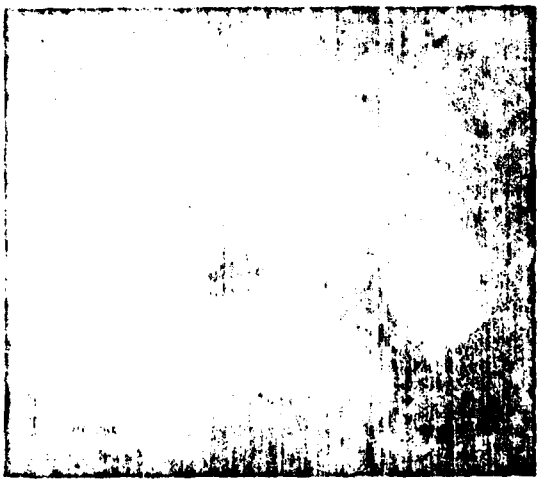

b

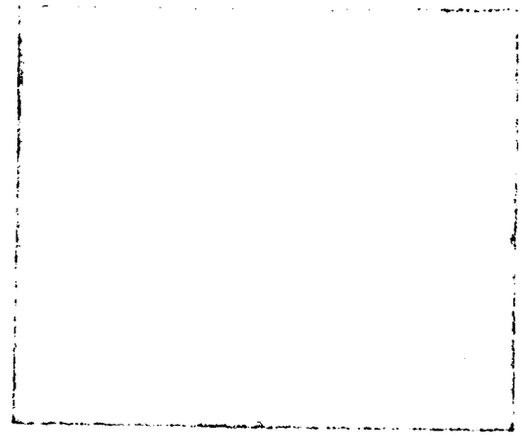

a

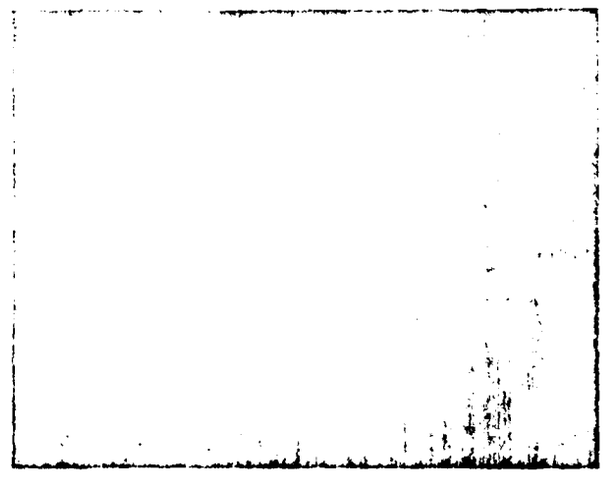

b

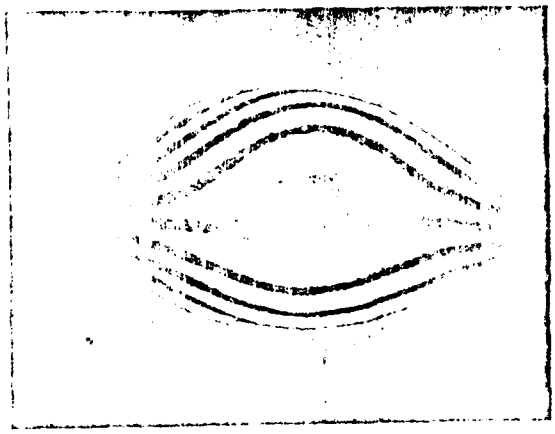

a

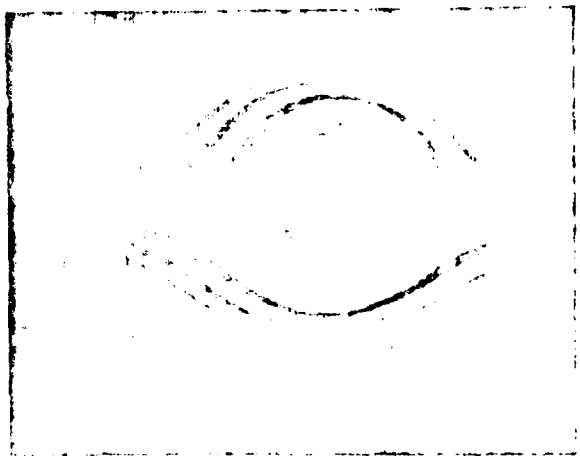

b

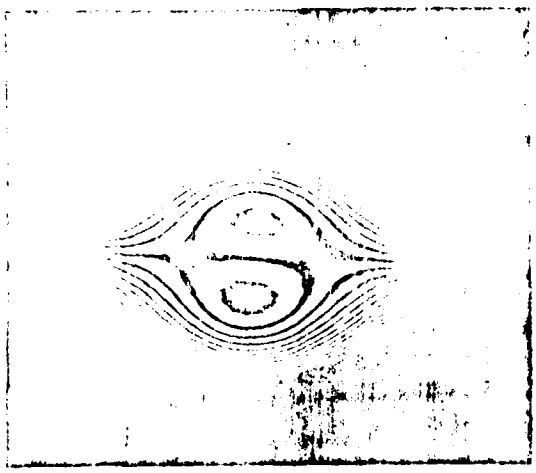

c

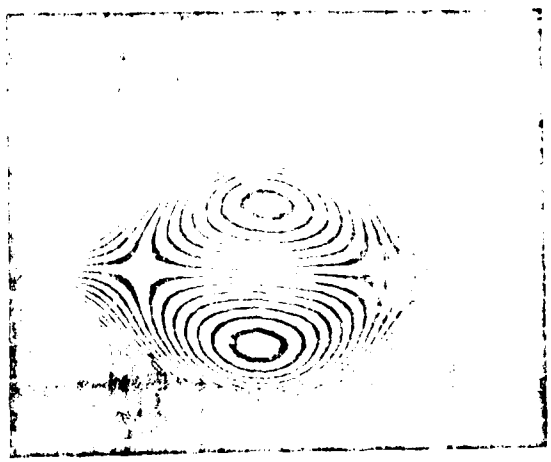

d

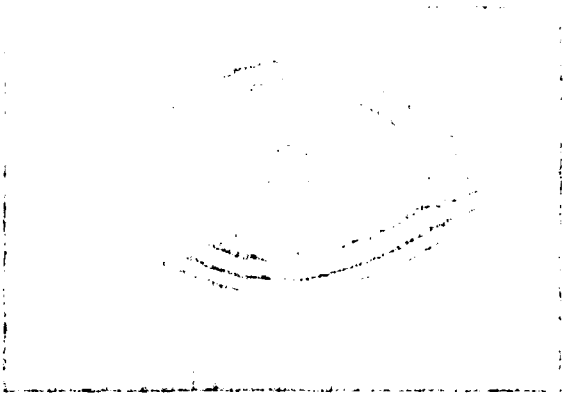

a

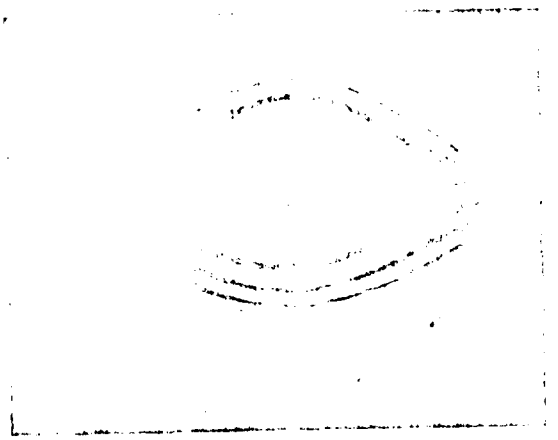

b

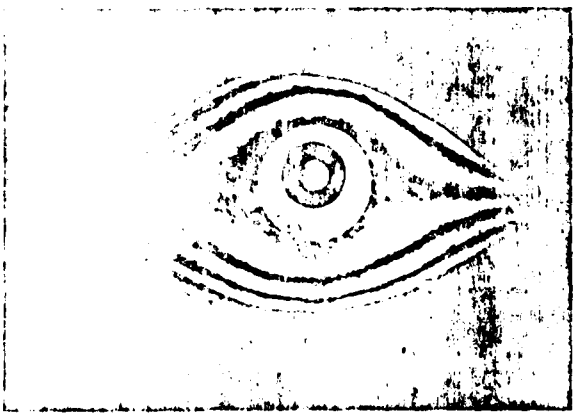

c

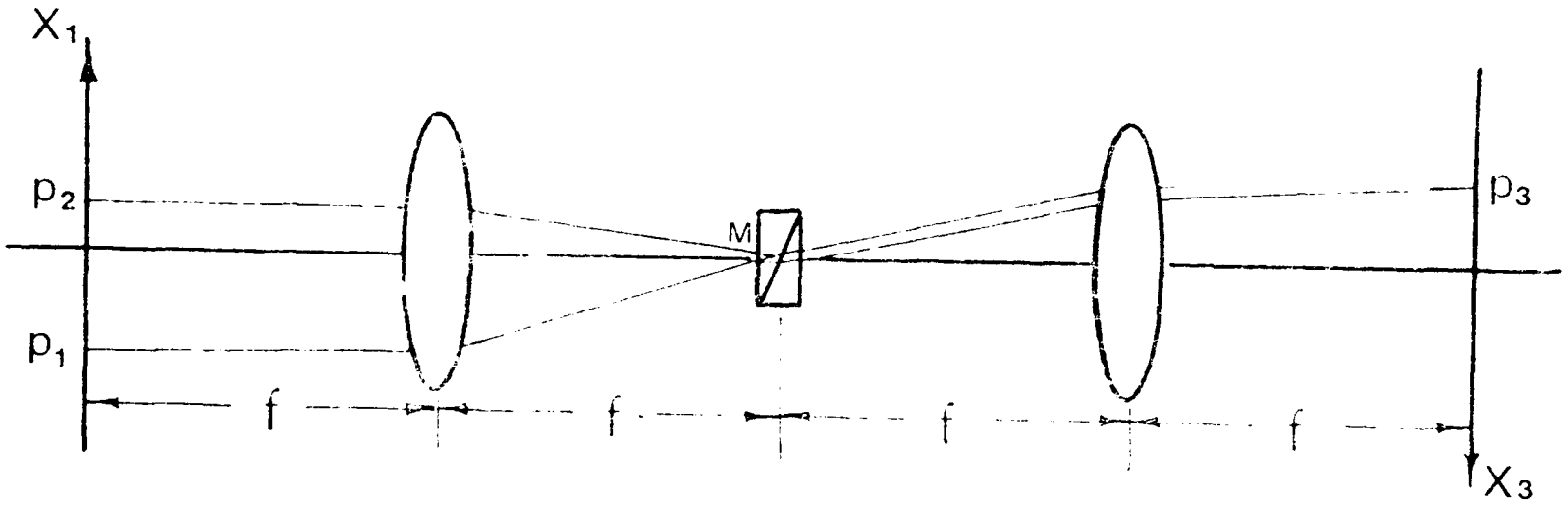
X1
p2
p1
M
p3
f
f
f
f
X3

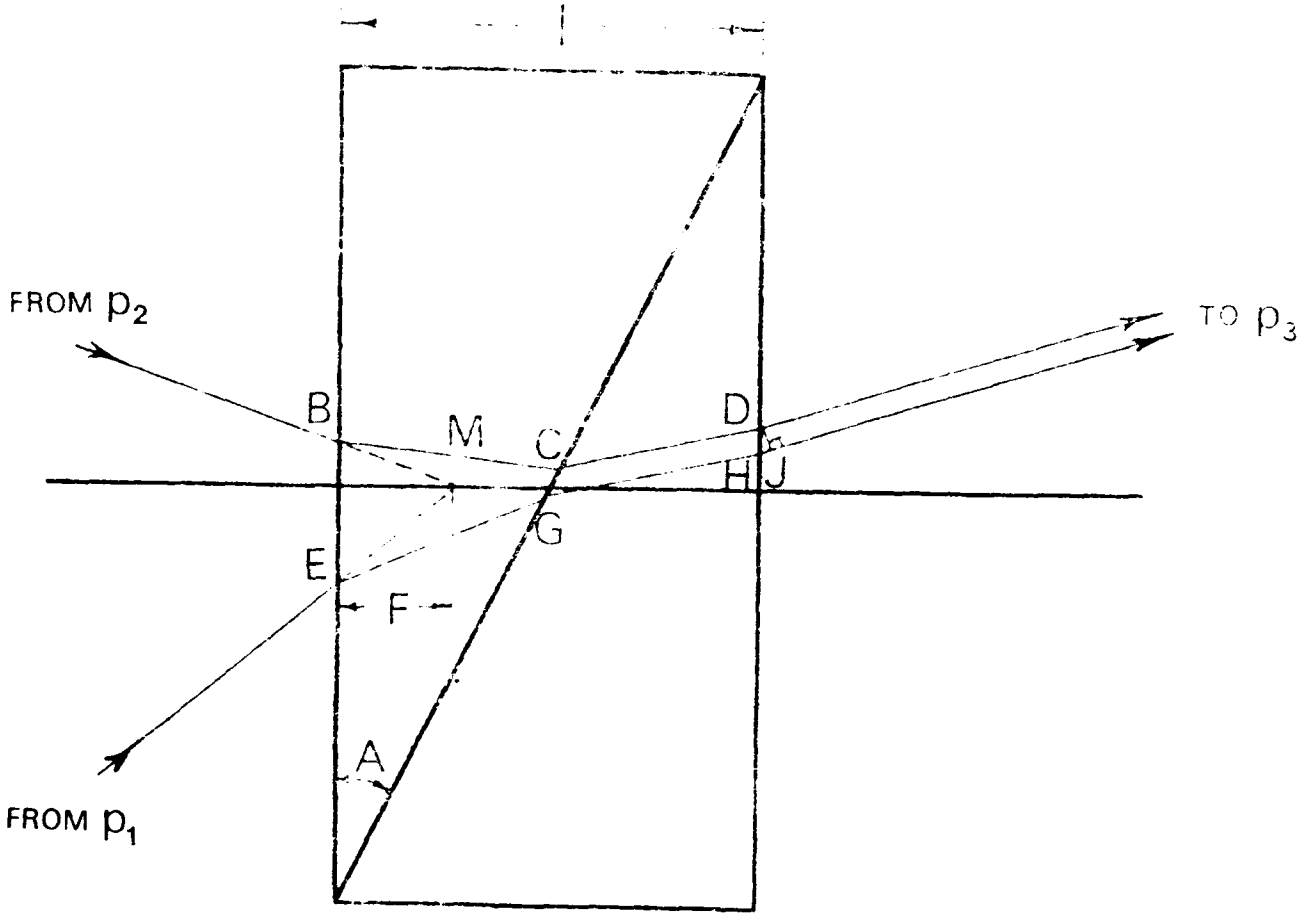
l
FROM p_2
TO p_3
B
M
C
D
H
J
G
E
F
A
FROM p_1

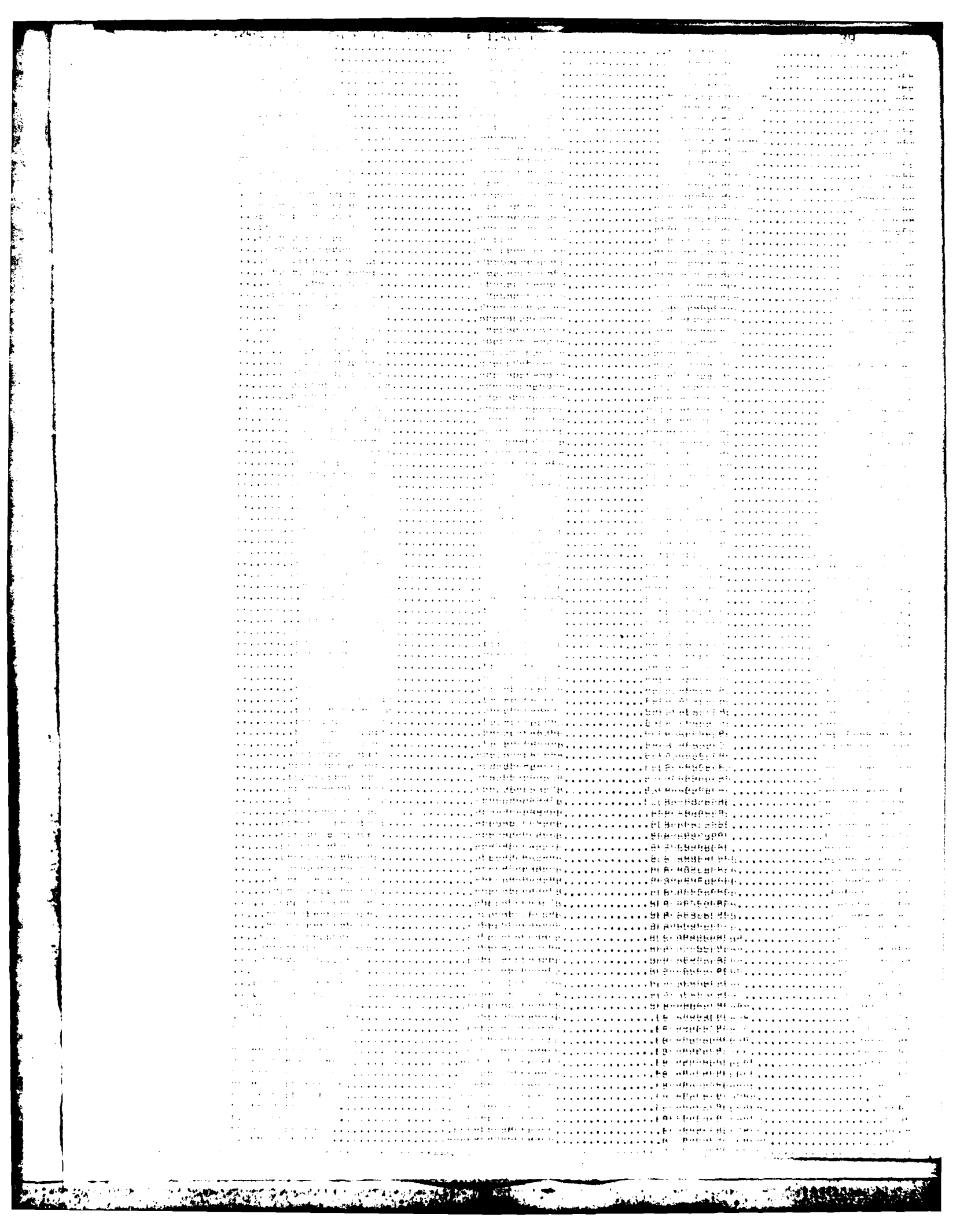

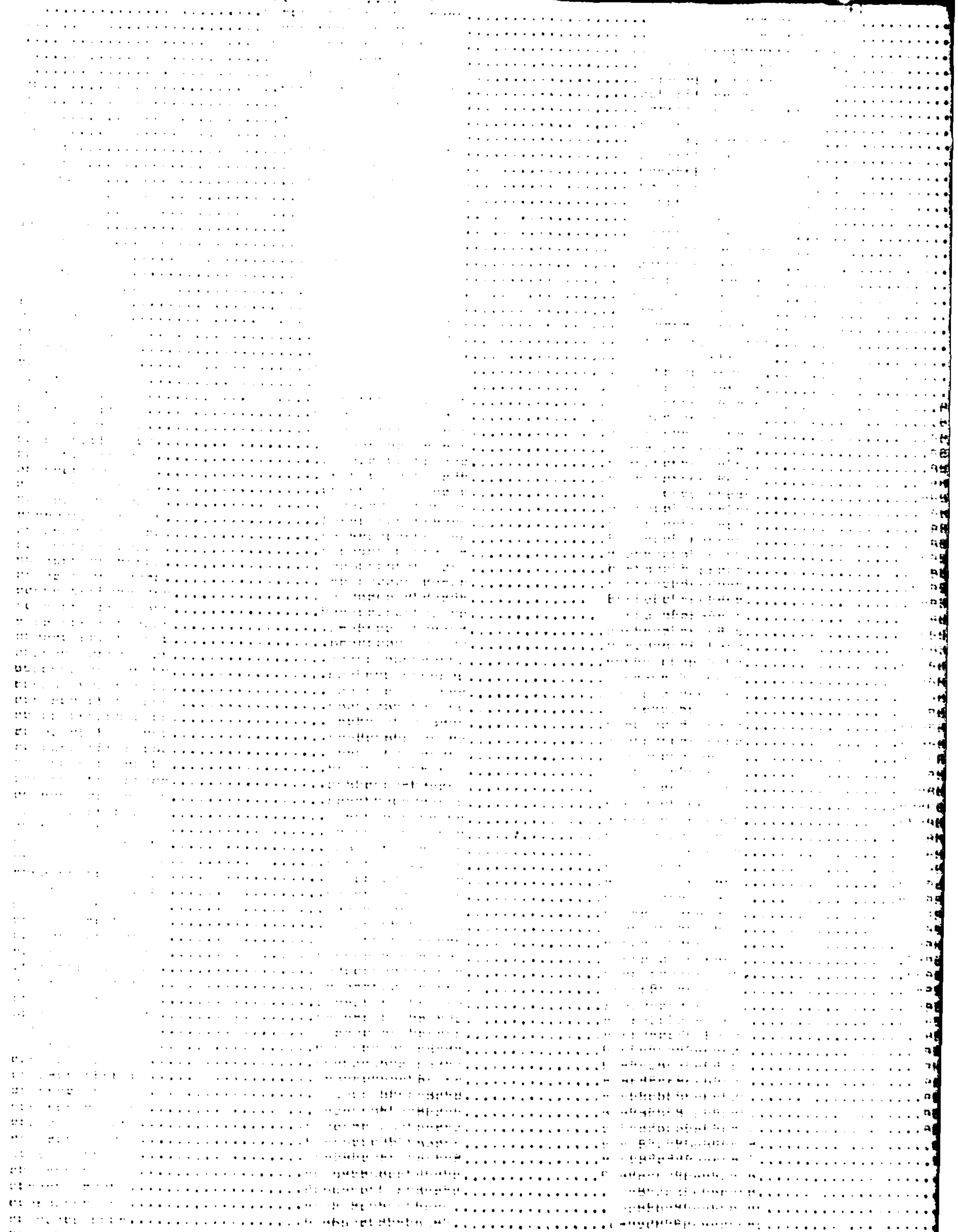

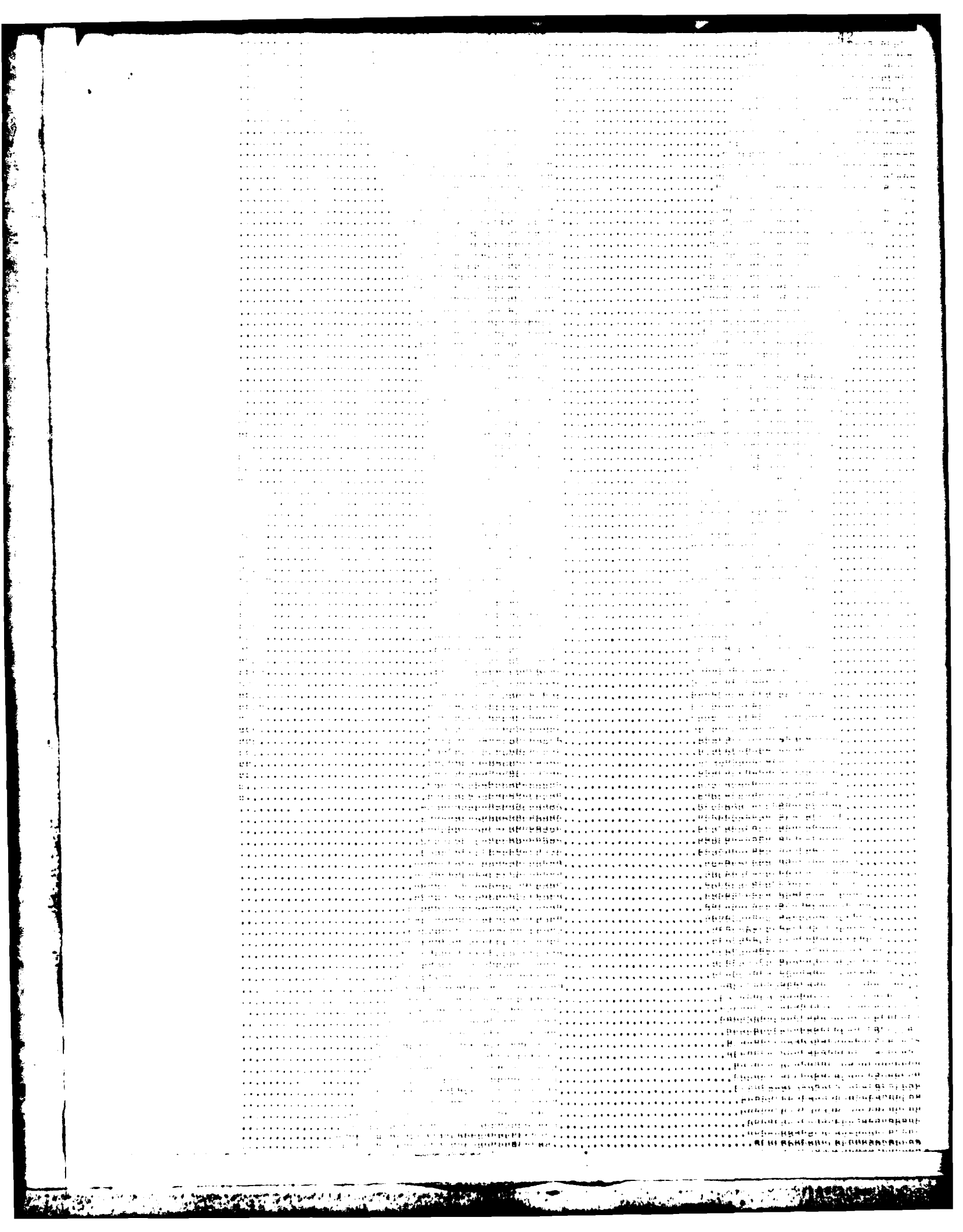

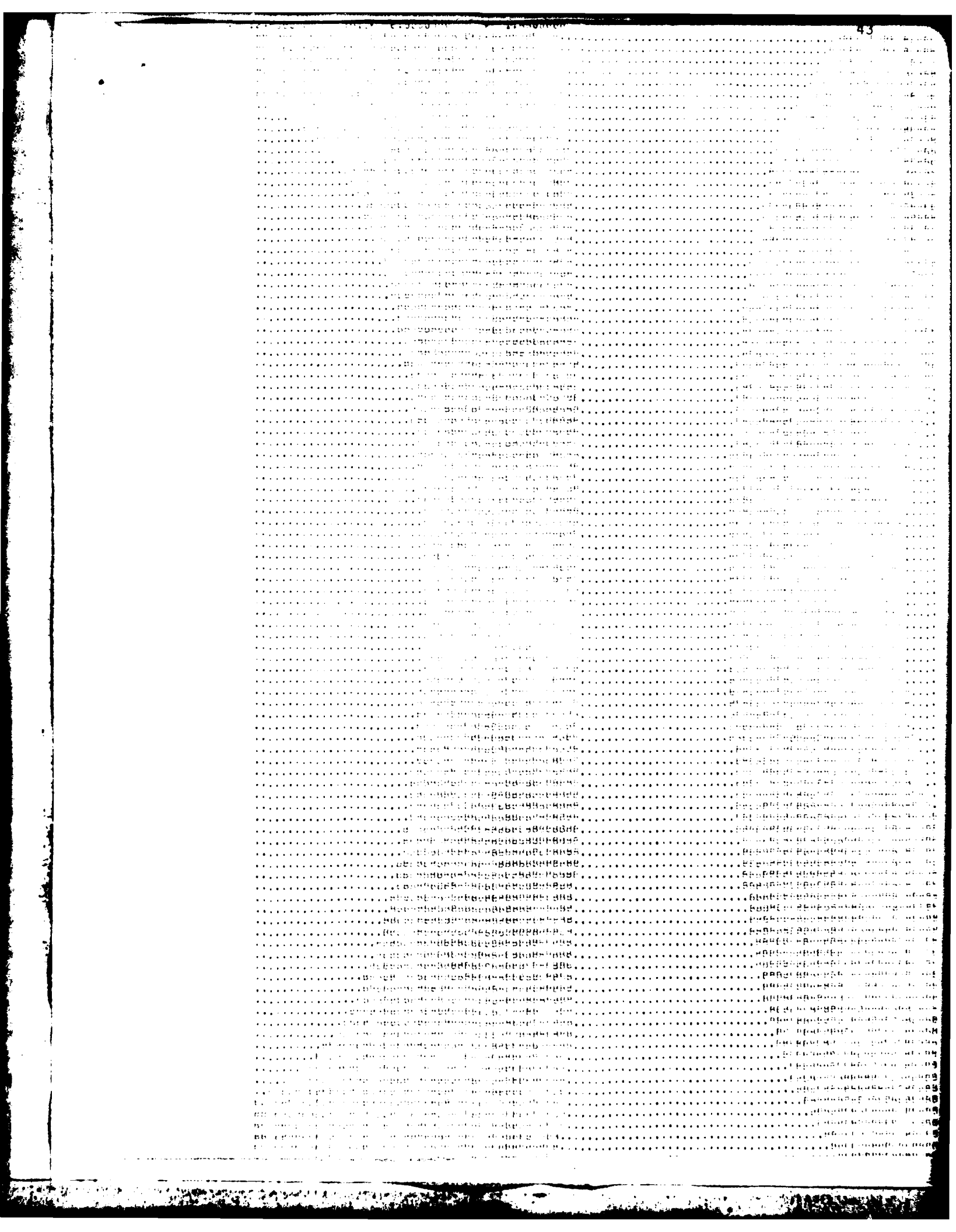

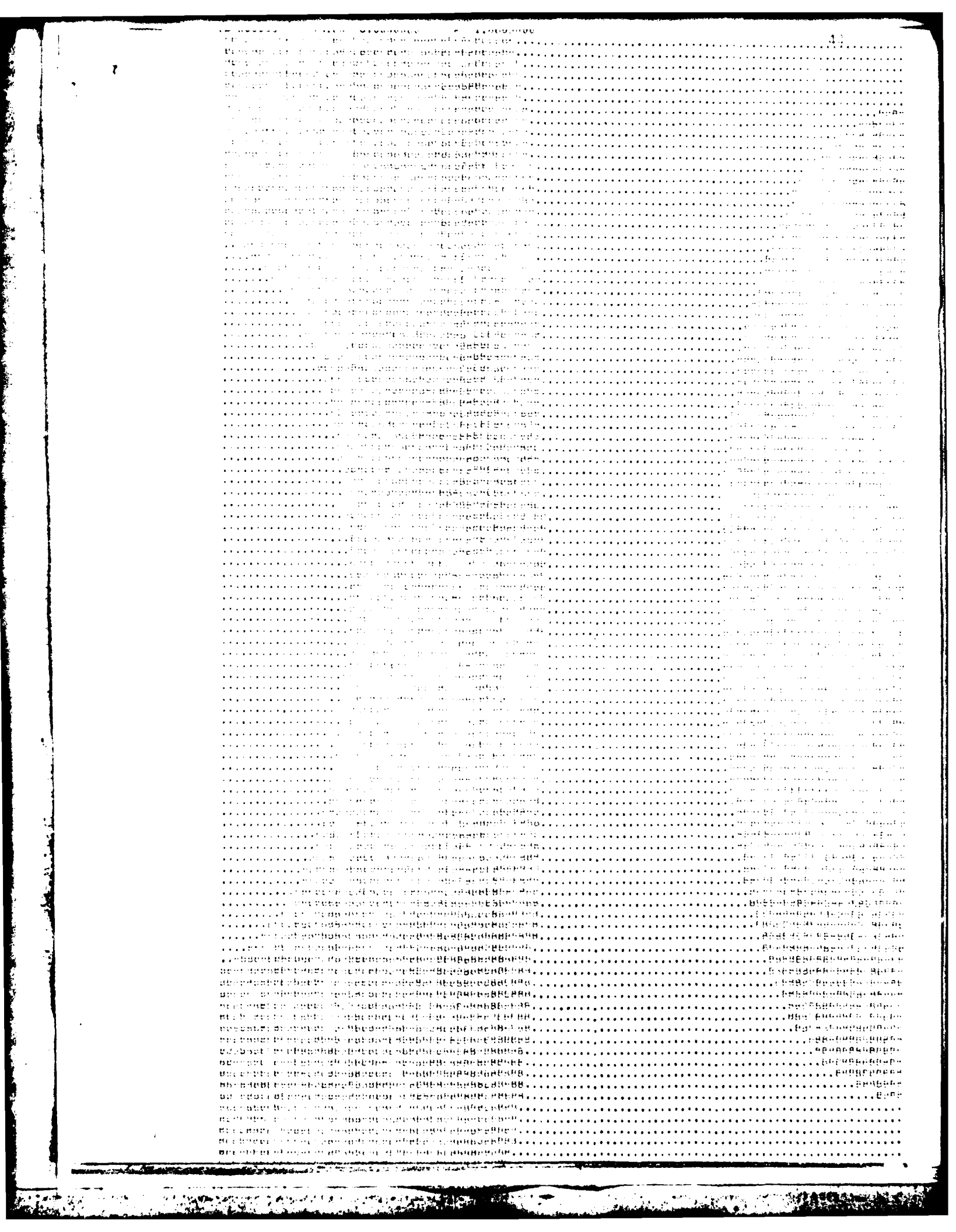

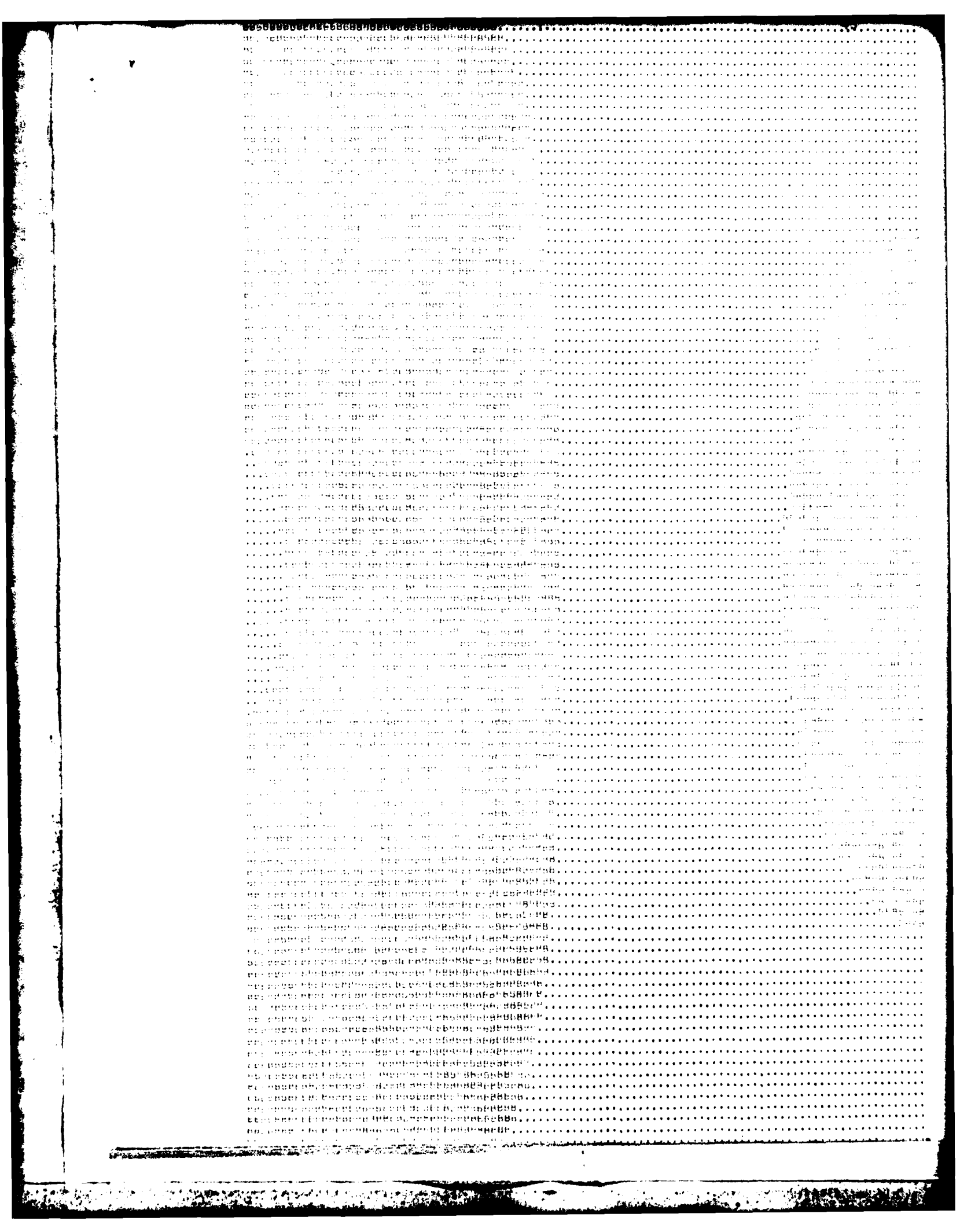

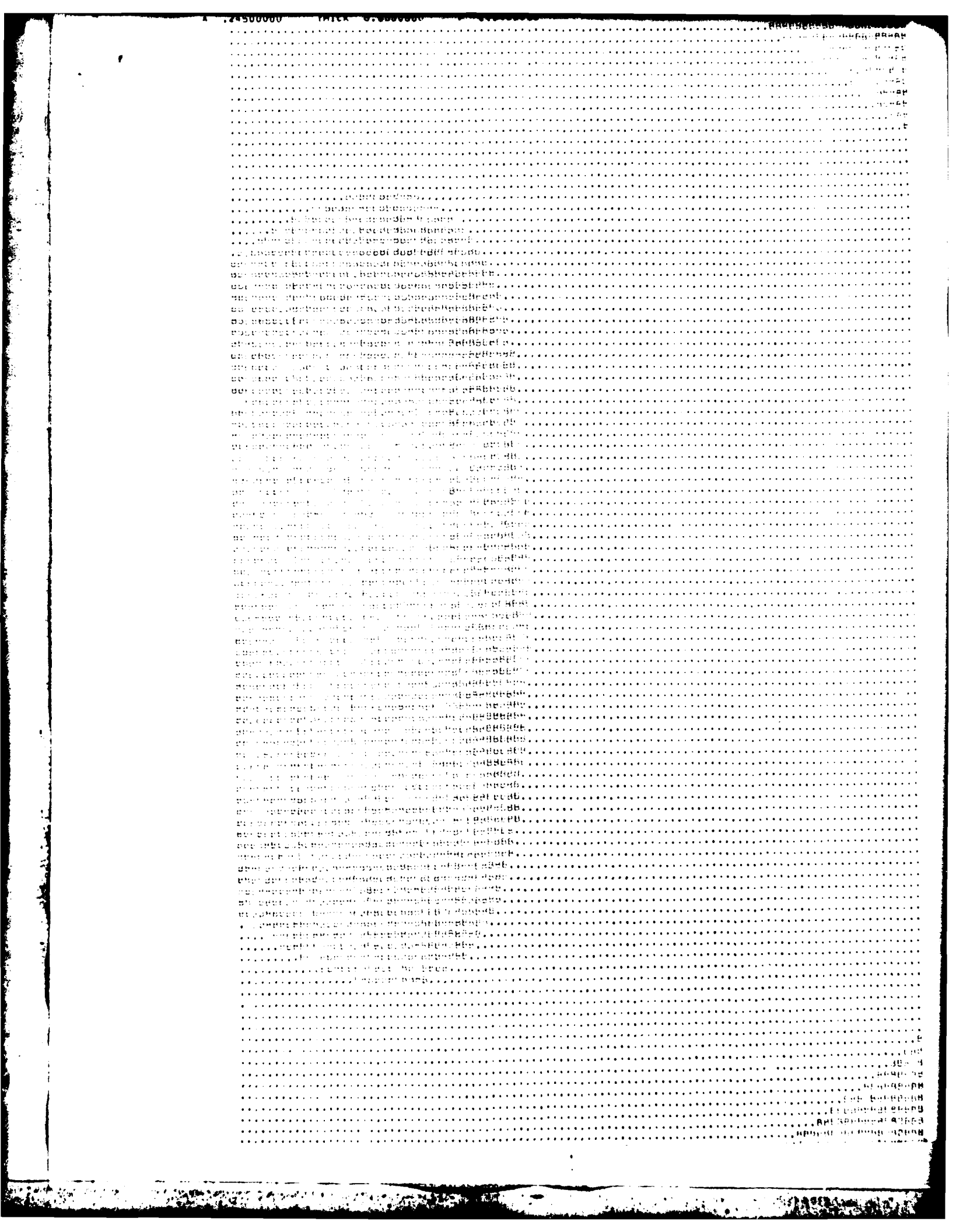

.24E+0... THETA ... F 1.9500+000

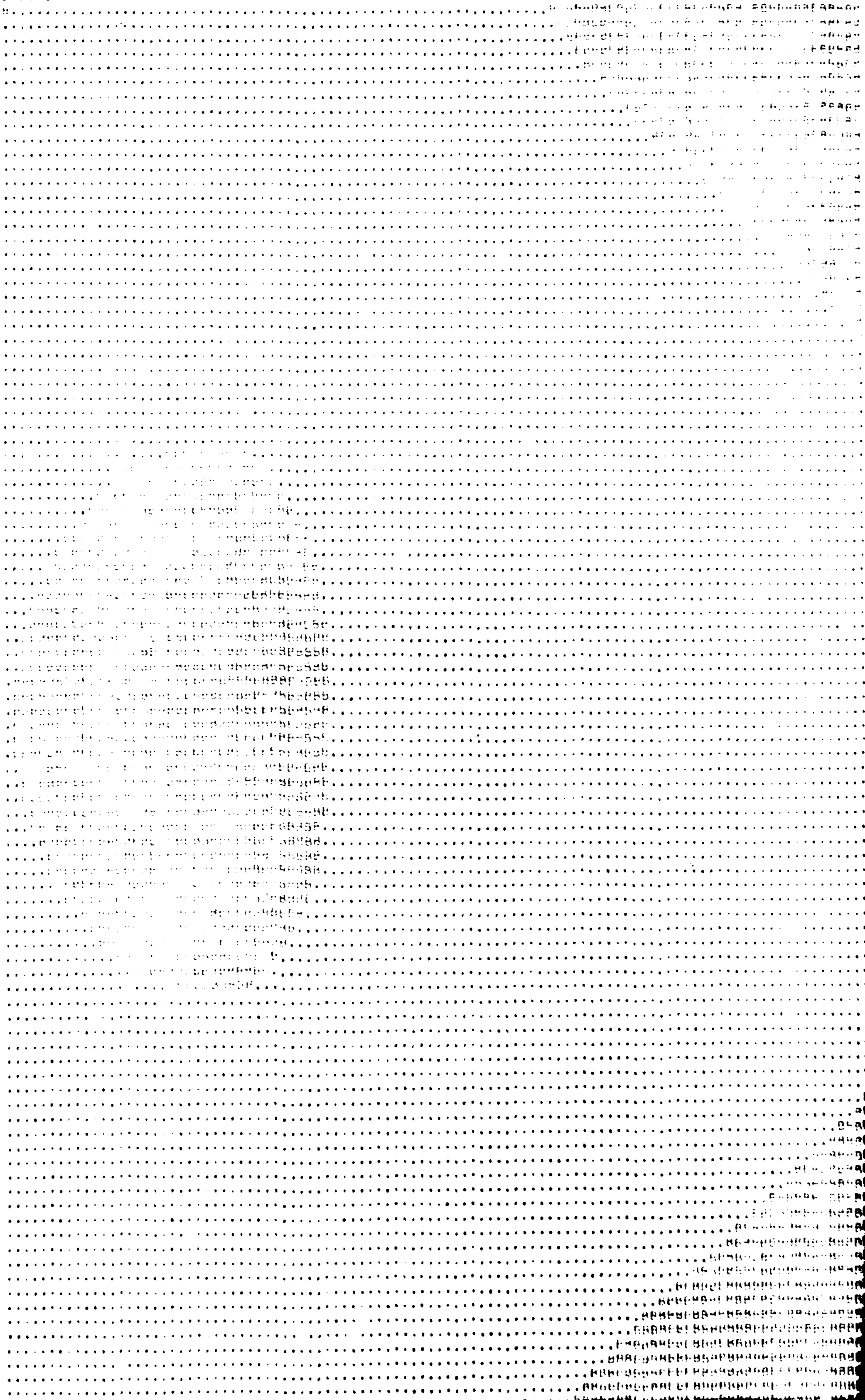

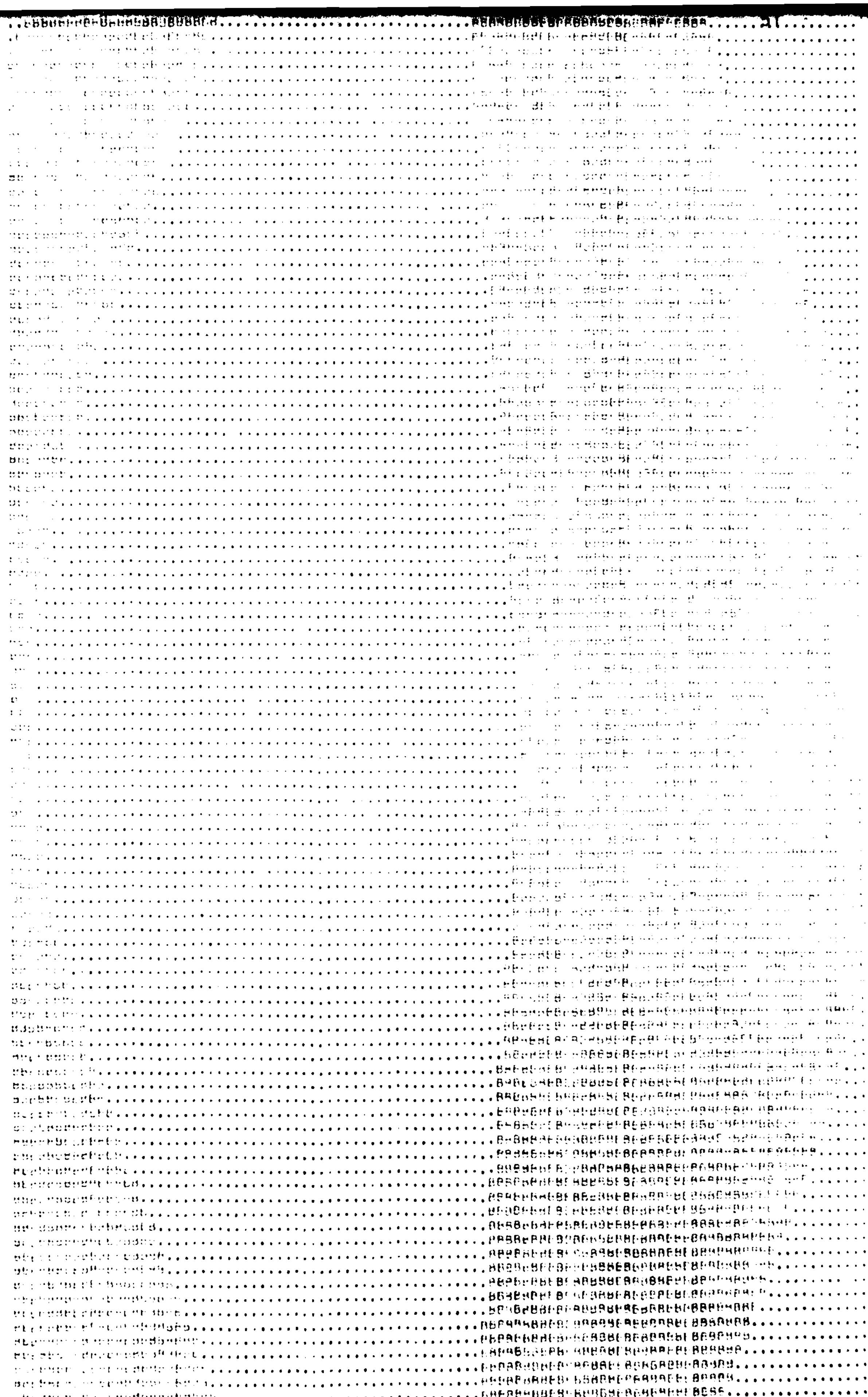

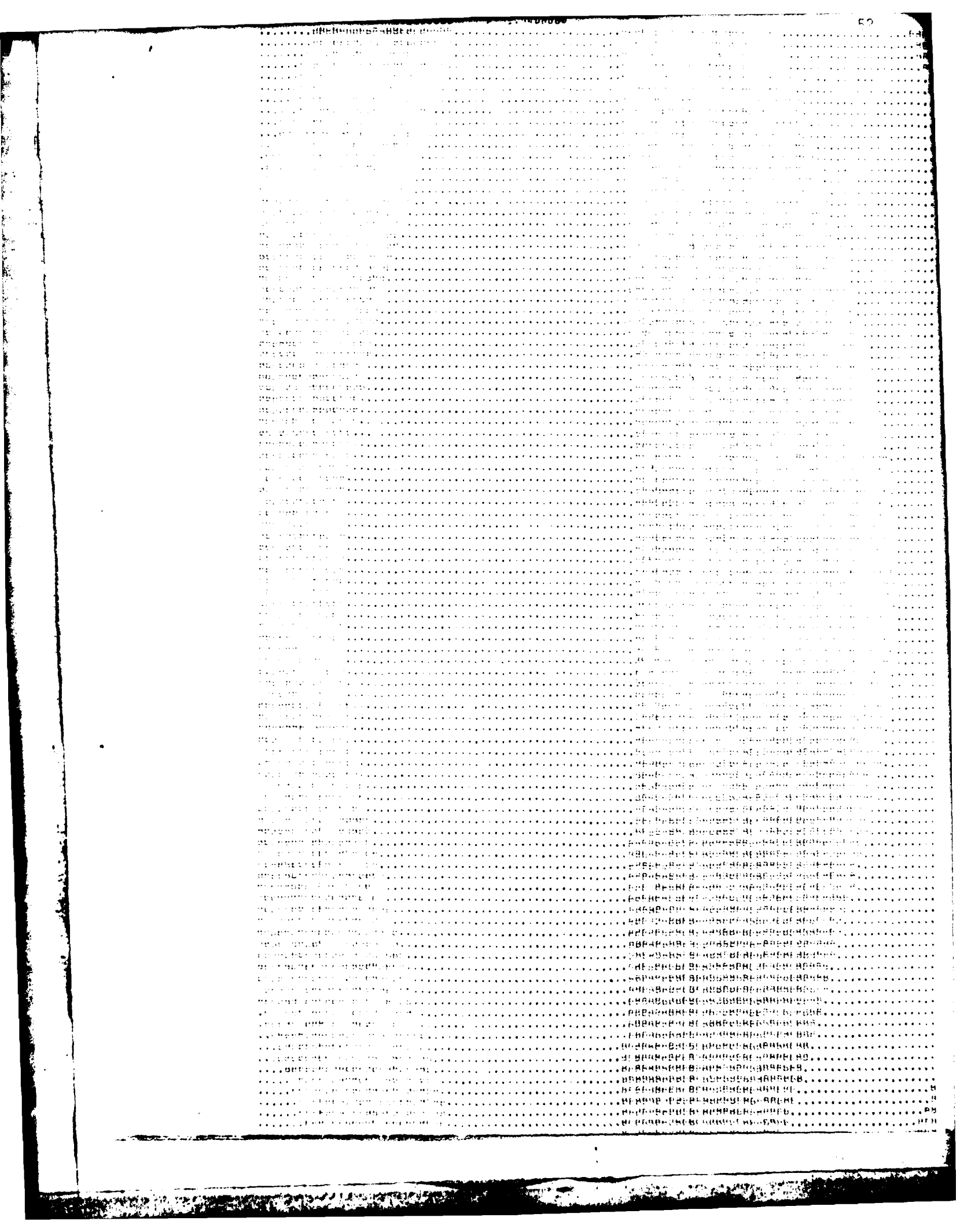

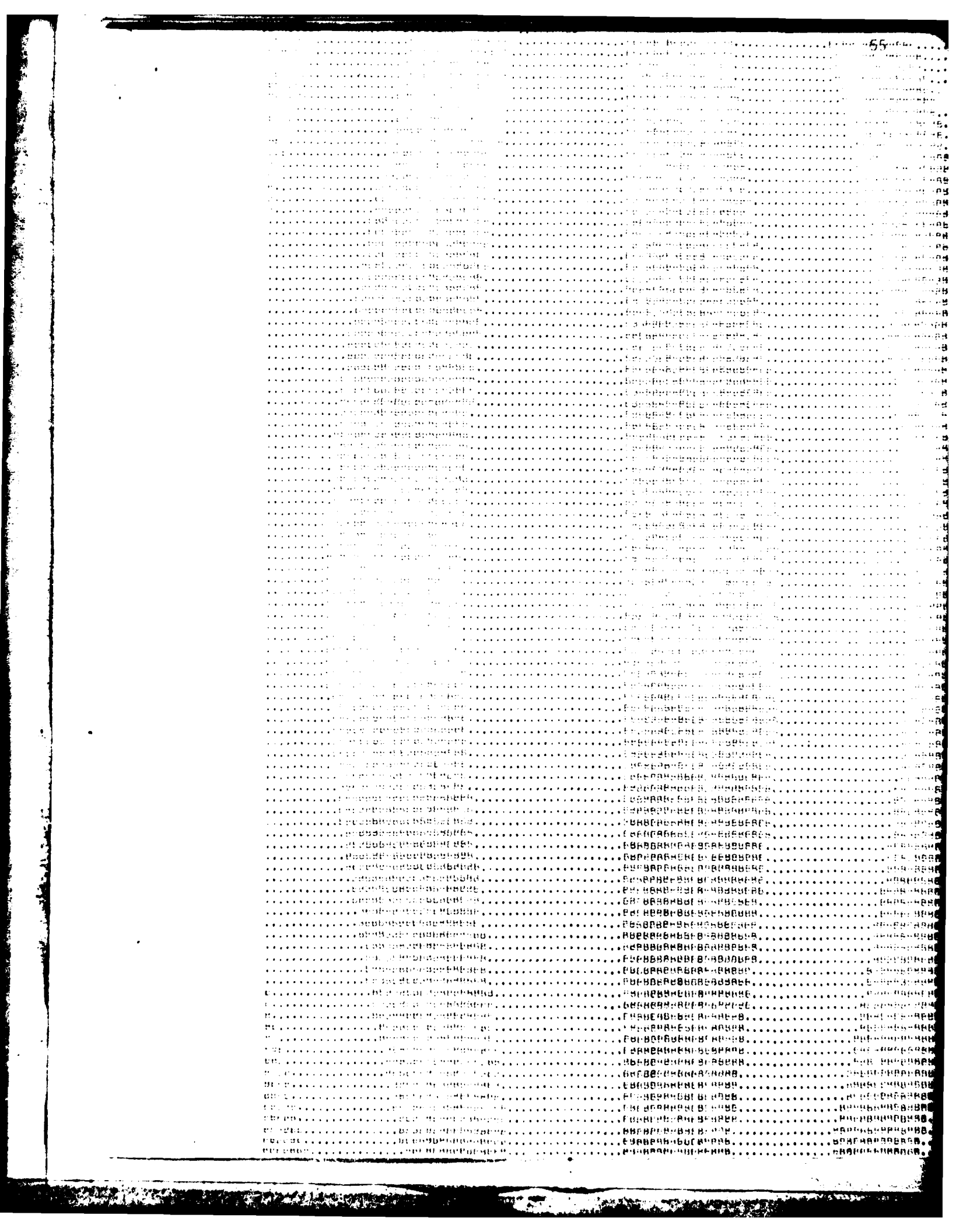

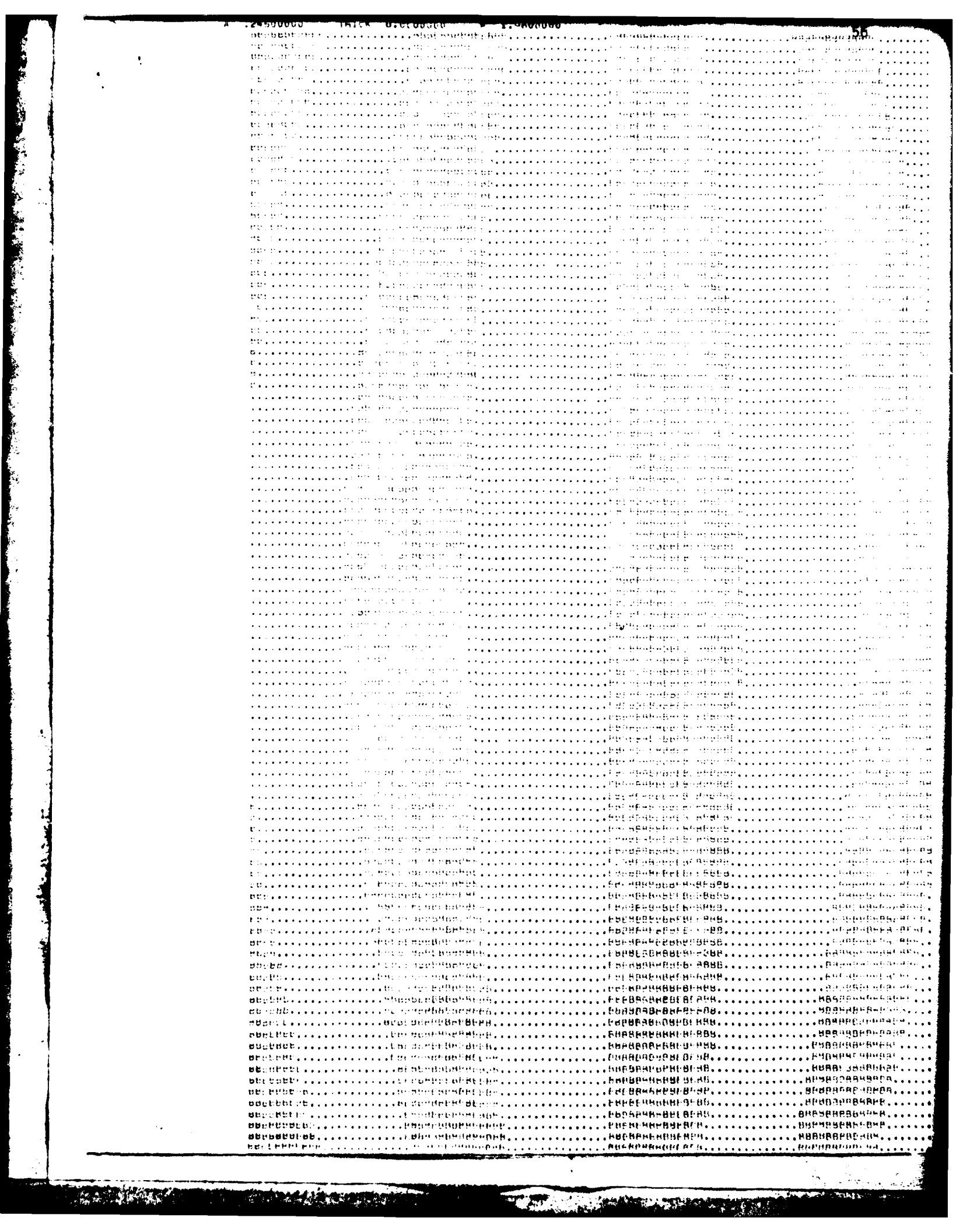

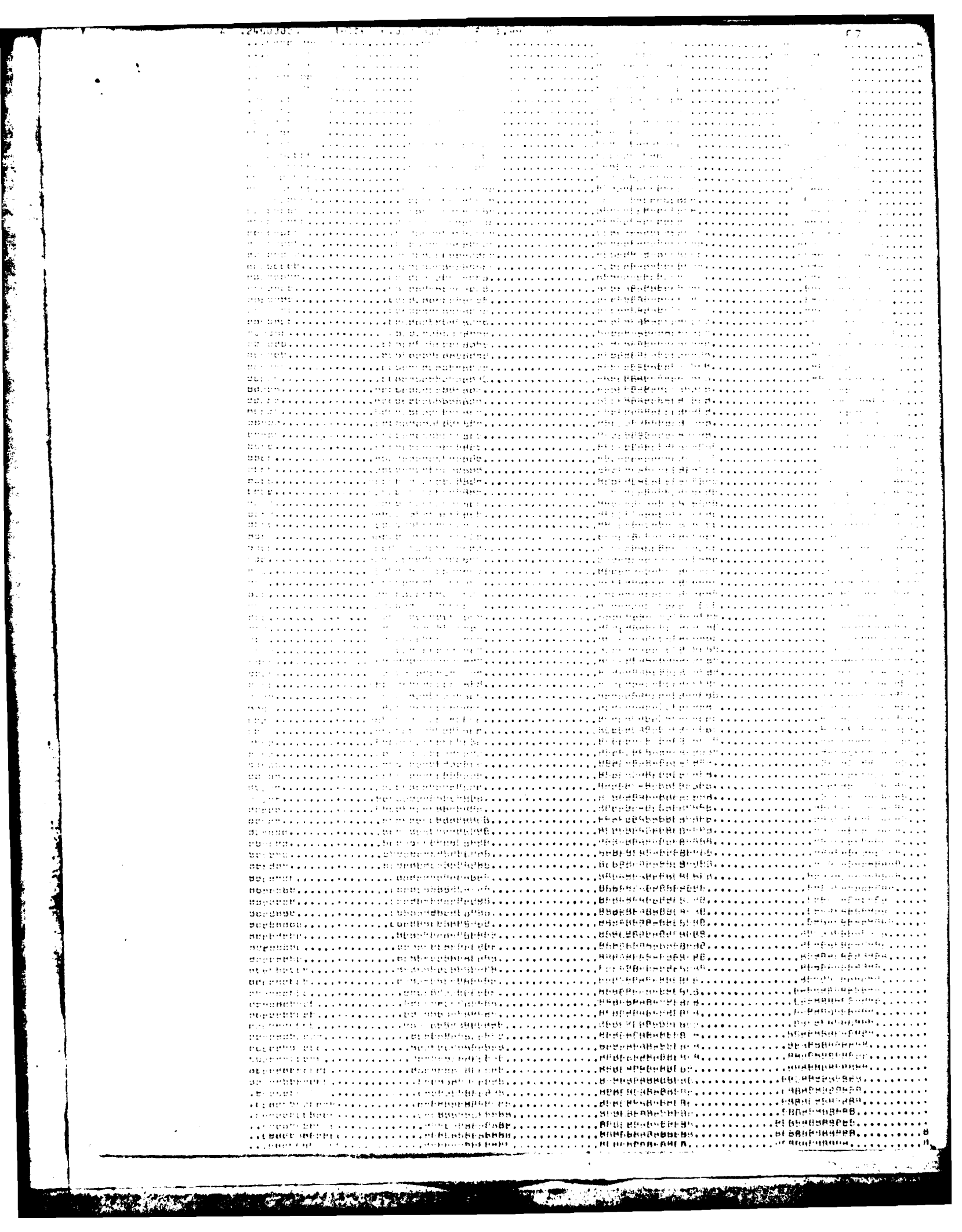

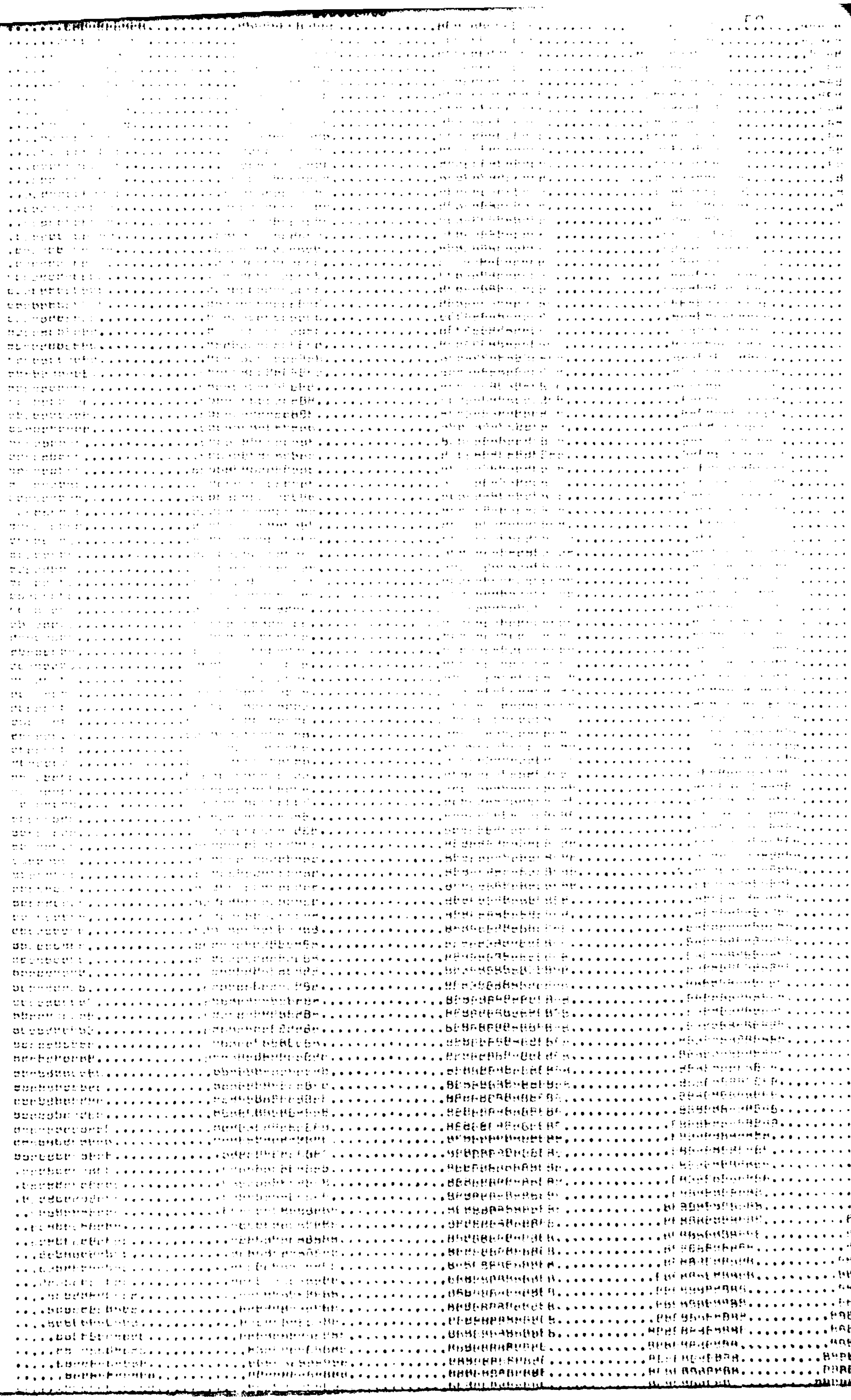

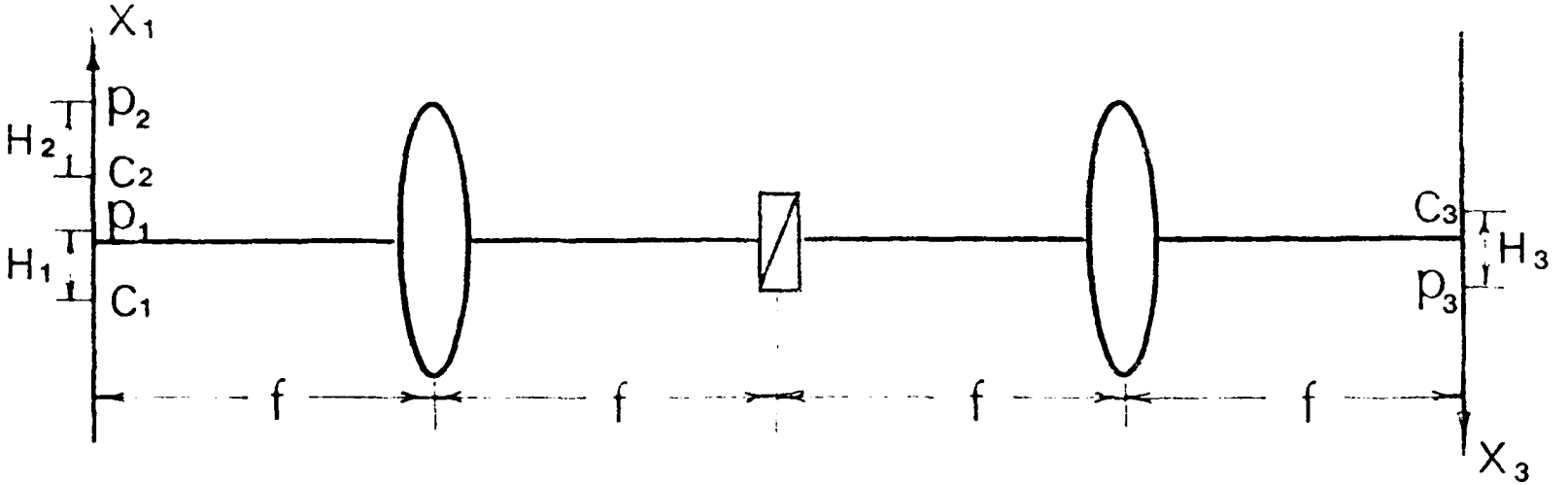
X1
p2
H2
C2
p1
H1
C1
C3
H3
p3
f
f
f
f
X3

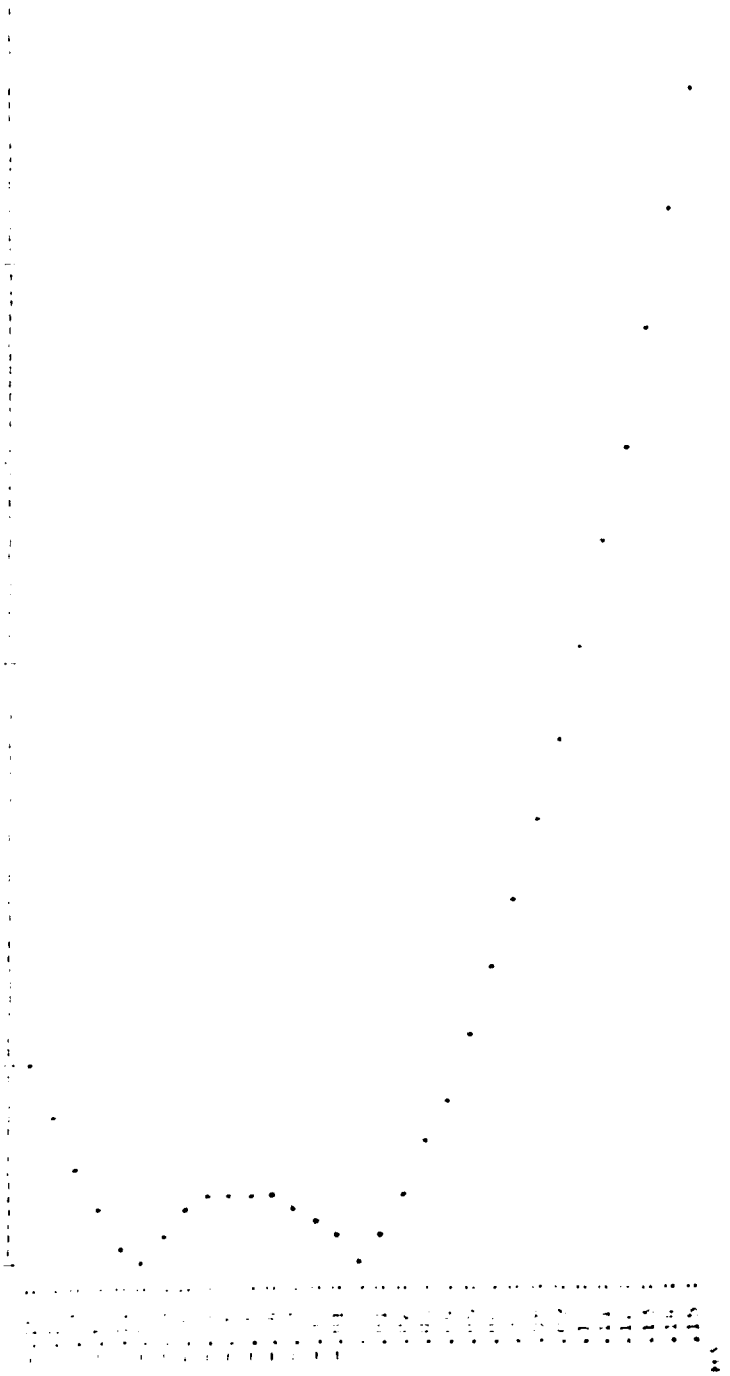

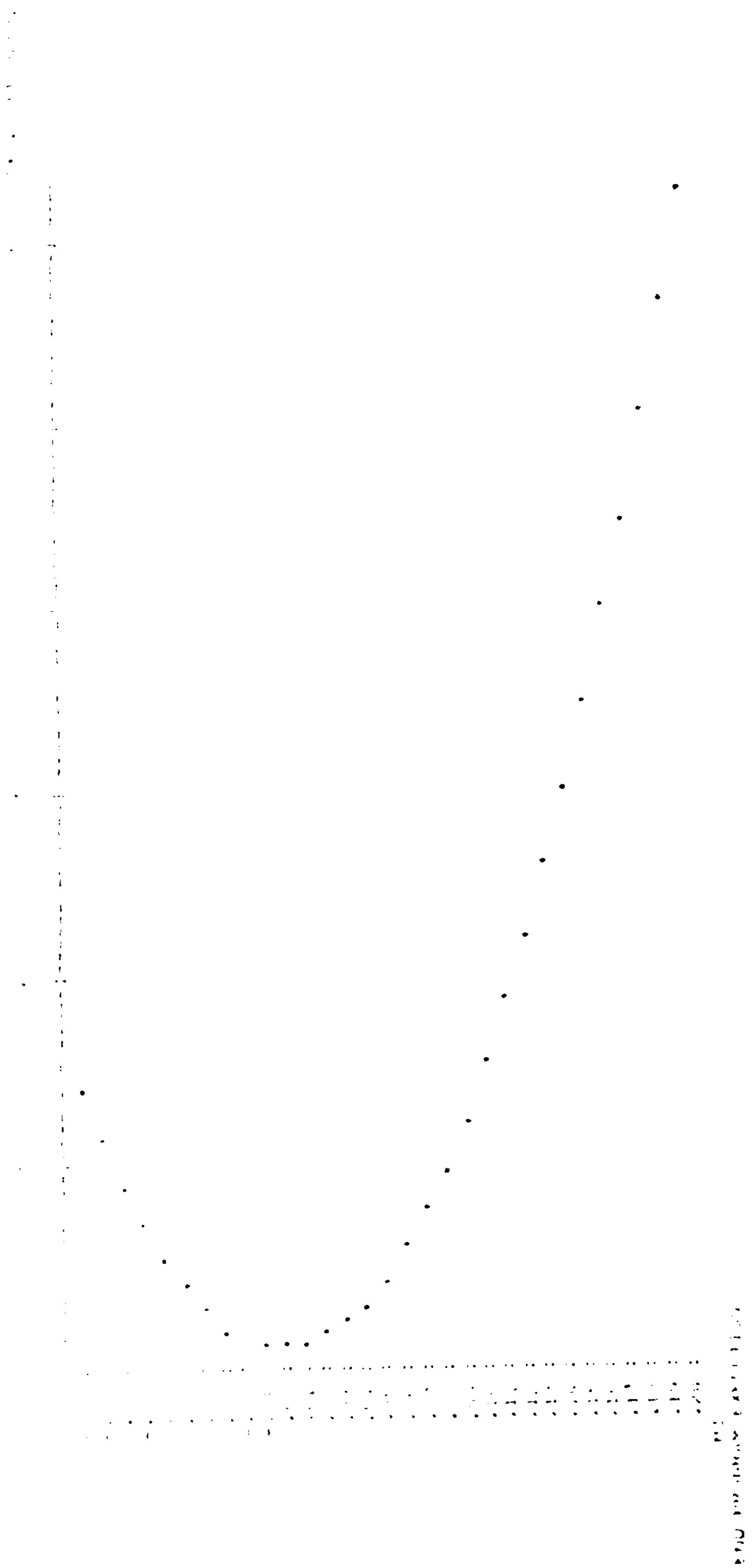

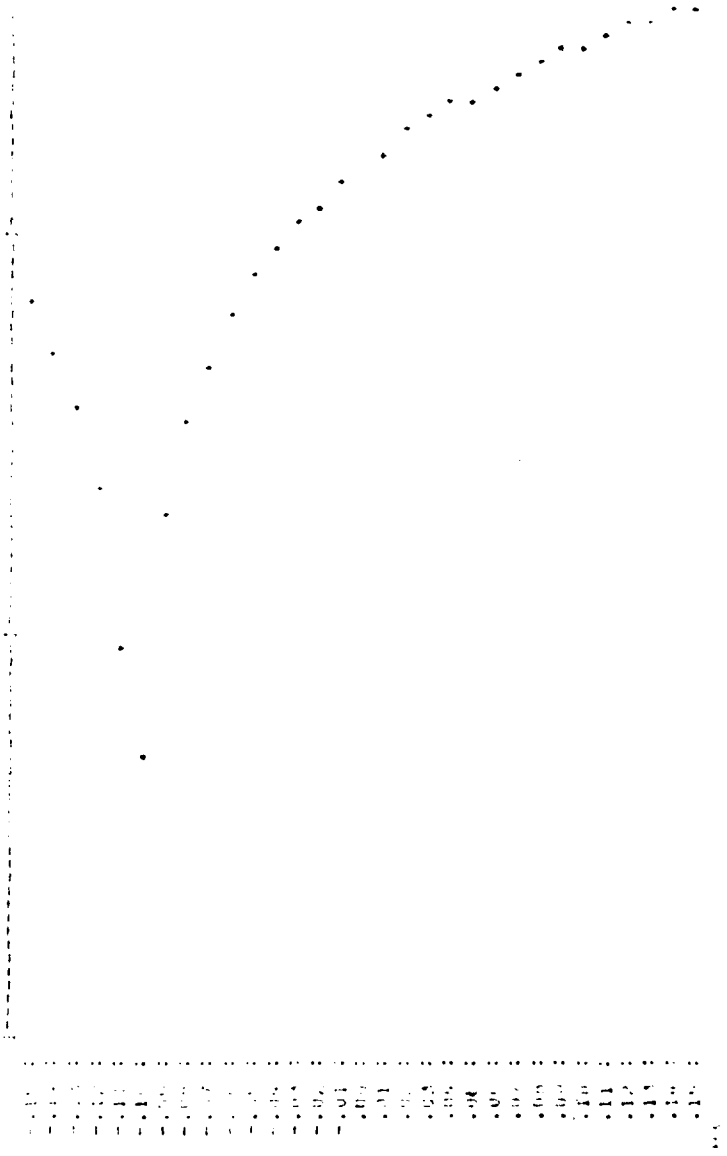

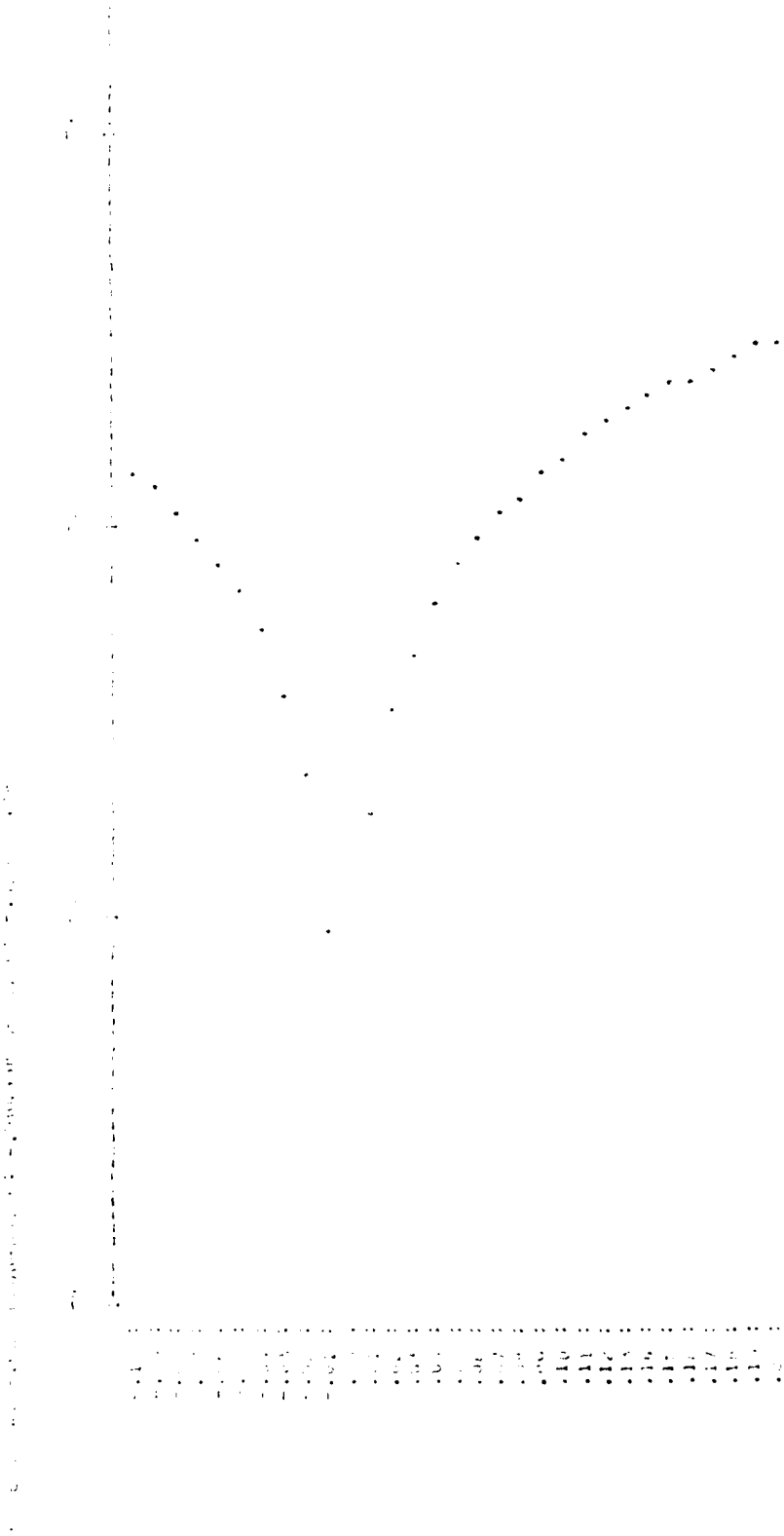

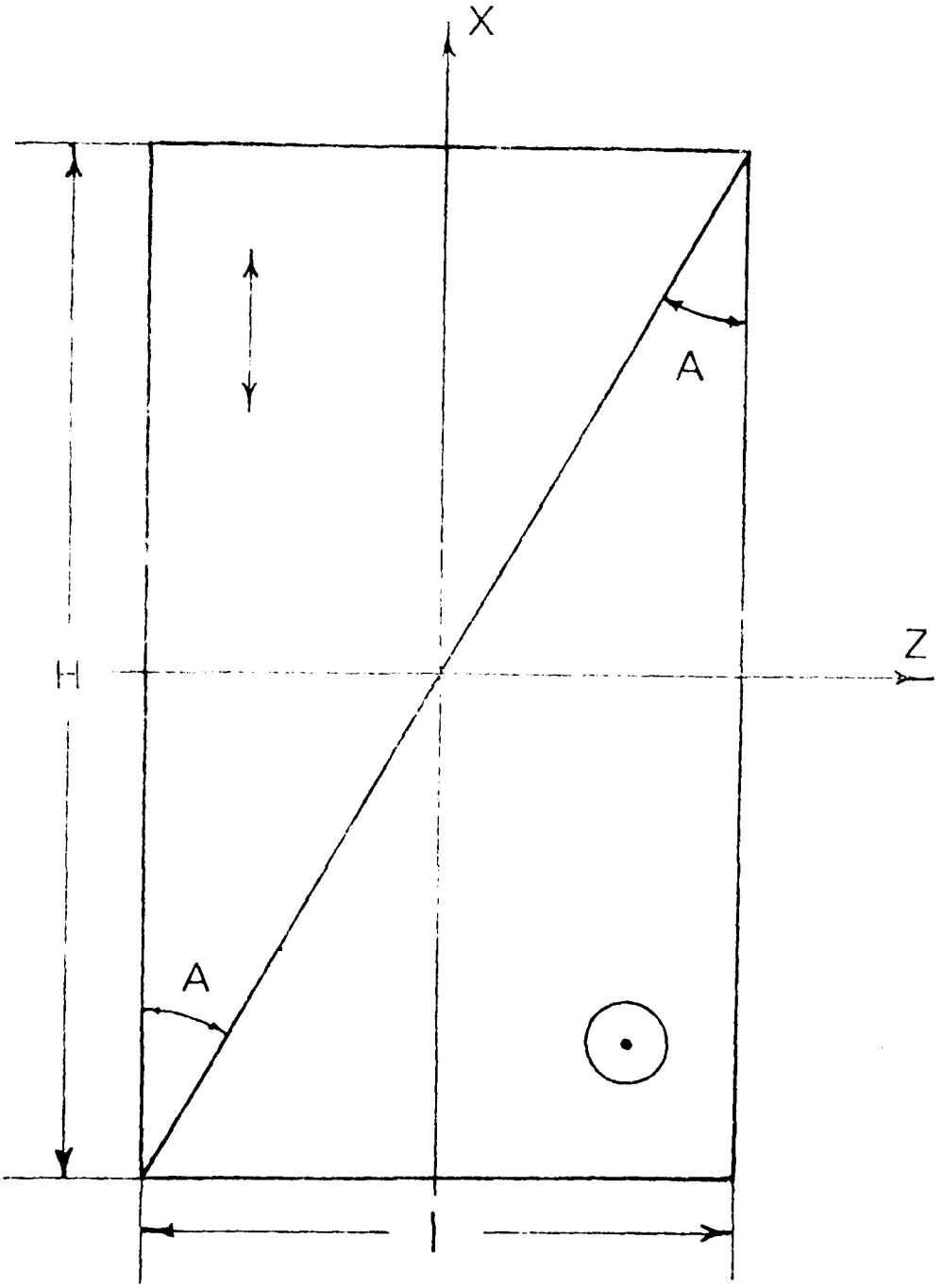
X
Z
H
A
A
l